63-1-1

AFCRL-62-701

S-459

RAYTHEON

RESEARCH ON THE CHEMISTRY AND SINGLE CRYSTAL GROWTH OF MAGNETIC OXIDES

H.J. Van Hook
A.E. Paladino
B.D. Roiter
R.L. Mozzi
T. Kohane

Research Division
Raytheon Company
Waltham 54, Massachusetts

Project 4608

Task 460803

FINAL REPORT

AF 19 (604)-8474

31 JULY 1962

Prepared for
ELECTRONICS RESEARCH DIRECTORATE
AIR FORCE CAMBRIDGE RESEARCH LABORATORIES
OFFICE OF AEROSPACE RESEARCH
UNITED STATES AIR FORCE
BEDFORD, MASSACHUSETTS

AFCRL-62-701

RESEARCH ON THE CHEMISTRY AND SINGLE CRYSTAL GROWTH OF MAGNETIC OXIDES

H. J. Van Hook

A. E. Paladino

B. D. Roiter

R. L. Mozzi

T. Kohane

Raytheon Research Division

Waltham, Massachusetts

Project 4608

Task 460803

Final Report

AF 19 (604)-8474

31 July 1962

Prepared for

Electronics Research Directorate

Air Force Cambridge Research Laboratories

Office of Aerospace Research

UNITED STATES AIR FORCE

Bedford, Massachusetts

Research on the Chemistry and Single Crystal

Growth of Magnetic Oxides

H. J. Van Hook

A. E. Paladino

B. D. Roiter

R. L. Mozzi

T. Kohane

ABSTRACT

Phase relationships in the liquidus range under different oxygen partial pressures are summarized for the system iron oxide-yttrium oxide, and detailed results of phase relations obtained by aluminum substitution in yttrium iron garnet are presented. Various methods of crystal growing are reviewed, and results of Czochralski growth of yttrium iron garnet are discussed.

Subsolidus phase relations are presented for the system FeO-Fe_2O_3-Al_2O_3. This system has been studied because of the interest in electrical conductivity processes in magnetite derived spinels. It allows for a trivalent substitution in Fe_3O_4, compared with the divalent substitutions such as Ni^{+2}, Co^{+2} and Mg^{+2}. Conductivity data obtained on samples of nickel substitutions in magnetite confirm a proposed model describing electrical conductivity in such systems. Cation distribution studies by X-ray intensity measurements and magnetic moment determinations have been made on the terminal composition of magnesium substituted magnetite and are reported.

TABLE OF CONTENTS

TABLE OF CONTENTS (Cont'd)

LIST OF FIGURES

LIST OF FIGURES (Continued)

LIST OF TABLES

LIST OF TABLES (Continued)

I. GENERAL INTRODUCTION

Experimental studies of crystal growth of ferromagnetic garnets and the chemistry of magnetic oxides have been the subject of three years research under this contract. The program can be divided into two areas: 1) liquidus equilibrium relations and single crystal growth in garnet-type oxide systems, and 2) subsolidus equilibria, electrical conductivity, X-ray distribution and saturation moment measurements in spinel type systems. These two larger categories can be divided into an initial phase of acquiring pertinent equilibrium data and a later phase where these results are applied in preparing known crystalline compositions under specific conditions. A knowledge of phase equilibria relations is particularly important in systems involving the transition metal oxides because of the large changes in oxygen content that occur at temperatures used for the preparation of polycrystalline and single crystal materials. Studies in this laboratory have dealt in detail with the thermal stability and chemical composition of certain magnetic oxide phases under variable conditions of temperature, oxygen pressure, and total cation content.

The data obtained in the garnet systems have been in support of a program on crystal growth from the melt and were confined primarily to the high temperatures where oxide liquids are stable. Phase equilibrium data obtained for systems containing ferrimagnetic spinels have been in support of a program of studying electrical conductivity in magnetite derived spinels. A simple model has been presented[1] to describe the valency exchange (Fe^{+2} - Fe^{+3}) conduction mechanism in one system, and this work is continuing beyond the termination date of this contract. The model should be applicable to many spinel systems, and its applicability is being tested on samples of explicitly defined composition, structure, and cation distribution.

II. GARNET SYSTEMS

A. Introduction

One objective of this study has been to evaluate the feasibility of growing yttrium iron garnet and related garnet compositions by crystallization directly from a melt of the constituent oxides. As part of this program, a detailed investigation has been made of the high temperature chemistry in several representative systems to determine the conditions of temperature, oxygen pressure, and composition required to produce garnet in stable equilibrium with oxide liquid. After a review of the techniques currently being used to grow the magnetic garnets,[2, 3, 4, 5] it was decided that a modification of the Czochralski or crystal pulling method was the most promising. Single crystalline boules of YIG have been grown by this technique in both a resistance heated furnace and an RF induction unit. The rate of crystal growth of sound material free from inclusions is somewhat slower using the resistance furnace, ~ 0. 004 cm/hr., compared to ~0. 04 cm/hr. using induction heating. The difference is believed to be due to higher temperature gradients at the growth interface in the latter case.

During the initial two-year contractual period, phase relations in the systems Y-Fe-O, Gd-Fe-O, and Y-Gd-Fe-O were investigated; this work has served as the basis for further equilibrium studies, and for early attempts at crystal growing of yttrium iron garnet using the resistance heated furnace. In the past year, work has continued along the same lines with additional phase equilibrium studies and further crystal growing experiments, but with greater emphasis on the latter. The factual data in this report include briefly the details of studies made during this last year on phase relations in a portion of the system Y-Al-Fe-O and on recent attempts at crystal growing.

B. Summary of the Systems Fe_2O_3-FeO-$YFeO_3$ and Fe-Y-Gd-O

A study of chemical equilibrium in the system iron oxide-yttrium oxide has served as the basis for all the work on crystal growing of yttrium iron

garnet and for further research on phase relations in more complex systems. Because of its critical importance, the system has been studied in greater detail than any of those that followed. The results are described in Scientific Report No. 1 (January 1960), No. 2 (January 1961), and in the Final Report (AFCRL 513, June 1961). They may be summarized as follows:

1. The compound yttrium iron garnet melts incongruently to yttrium orthoferrite and oxide liquid of the composition $Y_{0.44}Fe_{1.56}O_{2.88}$ at 1555°C in an air atmosphere (P_{O_2} = 159 mm Hg);

2. Addition of yttria to iron oxide lowers the melting temperature to 1469°C which is invariant in an air atmosphere, having the appearance of a binary eutectic. The liquid composition at this point has been determined to be $Y_{0.27}Fe_{1.73}O_{2.87}$;

3. Between the temperature limits of 1469°C and 1555°C, YIG can coexist in stable equilibrium with oxide liquid;

4. The composition of the garnet phase crystallizing from these iron oxide enriched melts at equilibrium does not correspond to the stoichiometric composition. Based on X-ray studies and weight loss measurements, the phase contains a small excess of iron and is slightly oxygen deficient. At 1469°C the YIG in equilibrium with "eutectic" liquid has a composition of $Y_{0.745}Fe_{1.255}O_{2.970}$ whereas at 1555°C the composition has changed to $Y_{0.745}Fe_{1.250}O_{2.960}$. The excess of iron oxide dissolved in YIG at 1470°C would result in the precipitation of about one percent of hematite if completely exsolved and oxidized at low temperature;

5. In an atmosphere of pure oxygen gas (P_{O_2} = 760 mm Hg) the minimum melting temperature is lowered to 1455°C and the decomposition temperature of YIG is raised to 1582°C, thereby increasing to 127°C the temperature range for the coexistence of garnet and oxide liquid;

6. In oxygen, the compositional changes in YIG with temperature are not significantly different from the changes in air. In both cases oxygen loss in YIG increases with temperature while solubility of excess iron decreases;

7. In the relatively reducing atmosphere given by the decomposition of pure CO_2 gas (P_{O_2} ≈ 1 mm Hg at 1500°C) the crystallization temperature range of garnet is reduced significantly. The composition of YIG appears to be near stoichiometric in metal atom ratio, but the phase is considerably reduced in oxygen content; at 1467°C with P_{O_2} = 1.1 mm Hg (CO_2 atmosphere) the composition is $Y_{0.745}Fe_{1.245}O_{2.945}$.

The study of the system iron oxide-gadolinium oxide was the first extension to compositions involving other magnetic garnet materials. Solid solubility was reported[6] to be extensive if not complete between gadolinium iron garnet (GdIG) and the yttrium iron garnet (YIG) as well as the corresponding yttrium-gadolinium orthoferrite phase. Since solid solution in the garnets can readily be followed by changes in lattice parameter and other physical properties, yttrium-gadolinium compositions seemed ideally suited to the investigation of the effect of a rare earth substitution for yttrium on melting relations. Previous work[7] indicated congruent melting for GdIG, and it was expected that this region of congruent melting would extend into the quaternary system. Investigation of the garnet region of the system Gd-Fe-O, however, indicated that GdIG melts incongruently and that the temperature range for coexisting garnet and liquid is even more restricted than that found in pure YIG. This is because GdIG decomposes in air at

1495°C to orthoferrite plus liquid, about 60°C lower in temperature than the corresponding reaction in YIG, whereas the air isobar eutectic temperatures are approximately the same. A series of compositions in the four-component system Y-Gd-Fe-O were prepared and the general melting relations investigated. The results, summarized in the final report, indicate incongruent melting for all garnet solid solutions of the form $(Y, Gd)_3Fe_5O_{12}$. There was no evidence for fractionation or change in the Y:Gd ratio during crystallization.

C. Phase Relations at Melting Temperatures in Aluminum Substituted Yttrium Iron Garnet

1. Substitutions in the Garnet Structure

In the garnet crystal structure there are three different cation sites each having a unique environment of oxygen ions: 1) the c-sites with a distorted eight-fold oxygen coordination, 2) the a-sites with octahedral or six-fold coordination, and 3) the tetrahedral d-sites. Taking the structure of yttrium iron garnet as a model, there appear to be three possible types of substitutions within size limitations which can be made for yttrium in c-sites and iron in a- and d-sites: a) direct substitution of other trivalent cations such as Gd^{+3} for Y^{+3} or Ga^{+3} for Fe^{+3}, b) paired substitution of ions of higher and lower cationic charge as $Ge^{+4} + Ca^{+2}$ for $Fe^{+3} + Y^{+3}$, and c) "unbalanced substitution" where cations with differing charge are accommodated by internal adjustments to obtain electrical neutrality, e. g., the presence of Si^{+4} favoring reduction of Fe^{+3} to Fe^{+2}. Anion substitution is also possible in any of the categories cited above, for example, the "unbalanced substitution" of F^- for $O^=$ in garnets could be accommodated by reduction of Fe^{+3} to Fe^{+2}.

A number of trivalent cation substitutions in yttrium iron garnet (YIG) have been reported by Geller[6] and by Bertaut and Forrat.[8] The substitutions which have been established experimentally are listed in Table I. Replacement of yttrium by any of the rare earth elements between atomic number 62 through 71 is apparently possible. One such rare earth substitution has been

TABLE I

Trivalent Cation Substitutions in Yttrium Iron Garnet[6]

c-sites	a-sites	d-sites
Y_3	Fe_2	Fe_3
↓	↓	↓
Elements 62 through 71 probably complete substitution.	Al_2 Ga_2	Al_3, Ga_3 — d-sited filled preferentially
↓	↓	
La, Pr, Nd — Limited substitution	Sc $(0 \le x \le 2)$ In $(0 \le x \le 1)$ Cr $(0 \le x \le 0.35)$	$Y_3\,[Fe_{2-x}M_x]\,(Fe_3)\,O_{12}$

studied in some detail, i. e., replacement of Y^{+3} by Gd^{+3} in the system Y-Gd-Fe-O.[9] A complete series of substitutional solid solutions are formed between yttrium and gadolinium iron garnet. Melting relations are remarkably similar for both end member garnets and for all intermediate compositions indicating that substitution of Gd^{+3} for Y^{+3} has very little effect on phase relations at liquidus temperatures. It seems reasonable to assume that the same general condition holds for other rare earth-iron garnets as well.

Only two elements, aluminum and gallium, are known to substitute completely for ferric iron in YIG. In both cases the replacement occurs preferentially in the smaller tetrahedral sites until essentially all positions are occupied.[6, 10, 11] Higher concentrations of Al^{+3} and Ga^{+3} result in replacement of octahedral Fe^{+3} in the garnet structure up to the end-member compositions $Y_3Al_5O_{12}$ and $Y_3Ga_5O_{12}$.

Scandium, indium, and chromium replace ferric iron to a limited extent in YIG.[6] Substitution is confined essentially to the octahedral cation sites. The solubility in all cases is below the limiting concentration where occupancy of the tetrahedral positions would be required. Scandium can replace ferric iron in octhaedral sites completely, whereas substitution of indium fills one-half of these sites at saturation and chromium substitution is limited to one-sixth of the octhaedral positions (see Table I).

In summary, the trivalent ion substitutions so far determined in YIG fall into three distinct categories: 1) complete replacement of rare earth ions for yttrium on c-sites, 2) complete substitution of aluminum or gallium for iron with a preference for d-sites at low concentrations, and 3) partial substitution of indium, scandium, and chromium for iron on the a-sites. A system which represents the first category has been previously studied;[9] the following describes the results of study on a system representative of the second, i. e., solid solutions of the type $Y_3Fe_{5-x}Al_xO_{12}$ where $0 \leq x \leq 5$ in the system Y-Al-Fe-O. The equilibrium study was undertaken to determine general stability relations between oxide liquid and the various crystalline

compounds especially the garnet phase. The equilibrium data could then be used to evaluate the extent of zoning in garnet solid solutions which was anticipated on the basis of the difference in ionic size of the cations Fe^{+3} and Al^{+3} which compete for the same lattice positions.

2. The Limiting Systems, Y-Fe-O, Fe-Al-O, Y-Al-O

Previous studies have been made of the garnet region of the system Y-Fe-O.[12] The experimental results for the air isobar in this system are shown in Fig. 1. In the lower diagram composition is indicated in terms of starting mixtures without regard to oxygen loss. The actual oxygen fraction of the condensed phases is shown in the triangular plot immediately above the binary projection. In the air isobar, addition of yttria to iron oxide lowers the melting temperature to a minimum value of 1469°C. The garnet phase melts incongruently at 1555°C to orthoferrite plus an iron oxide rich liquid. Within this temperature range garnet and oxide liquid phases coexist under equilibrium conditions.

The second limiting system, Fe-Al-O, has been investigated by Muan and Gee[13] and others.[14, 15] The diagram given by Muan and Gee is reproduced in Fig. 2, which is a binary projection of the air isobar with ternary composition shown in the triangular diagram. The addition of alumina to iron oxide raises the melting temperature range of the spinel solid solutions up to a limiting spinel composition of approximately $Fe_{0.9}Al_{2.1}O_{4.2}$ (point d) at 1710°C. Note that this terminal composition exceeds the 2:1 ratio of Al:Fe in hercynite and that the spinel is cation deficient (contains excess oxygen). At higher temperatures the primary crystallization field corundum plus liquid dominates liquid relations.

The third limiting system, Y-Al-O, has been studied briefly by Warshaw and Roy.[14] Their data indicate congruent melting for the yttrium aluminum garnet (YAG) at approximately 1970°C. A second congruently melting phase, $2\ Y_2O_3 \cdot Al_2O_3$, was also reported. The orthoferrite phase $YAlO_3$ was found to be metastable at high temperatures and does not appear in the diagram.

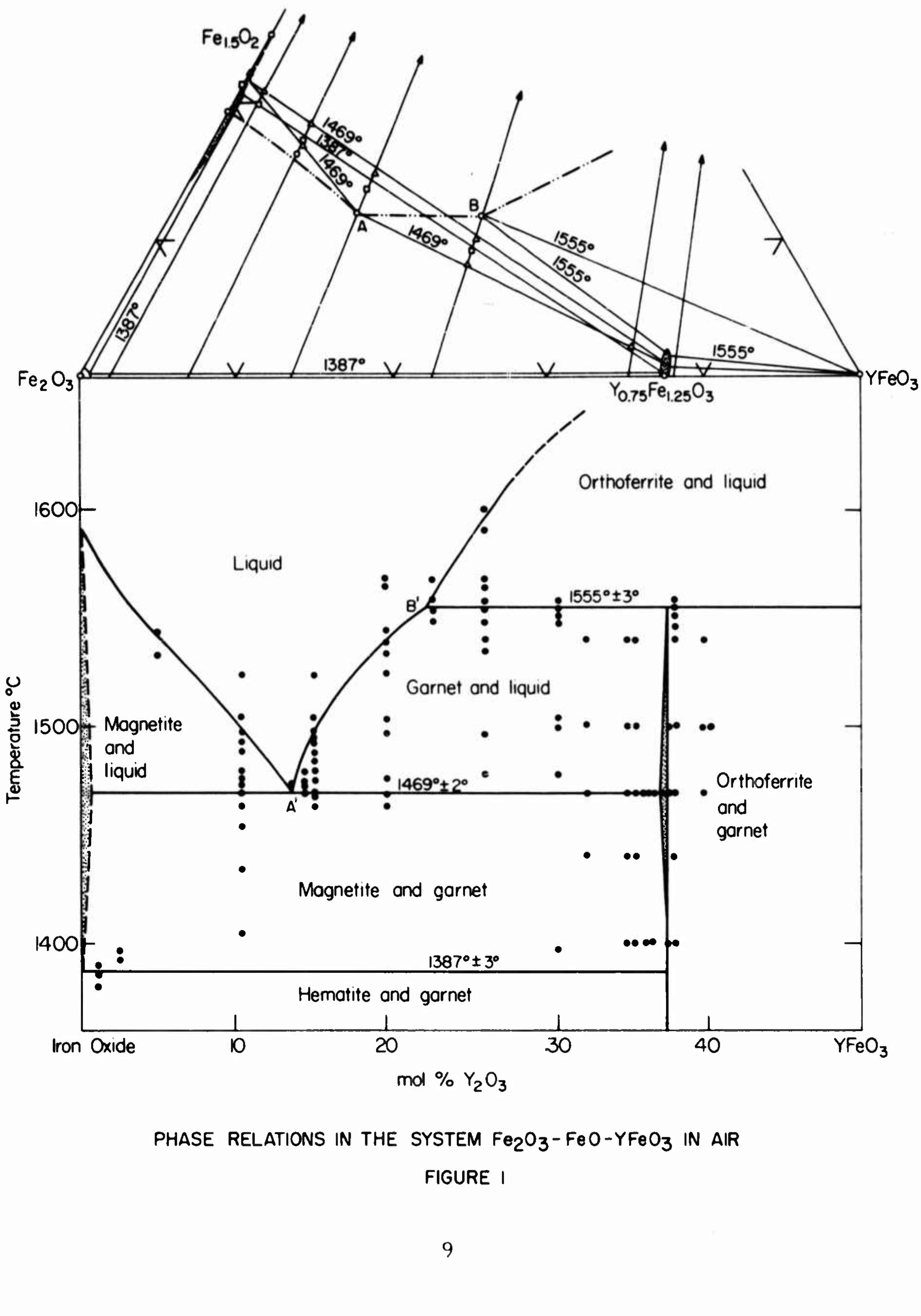

PHASE RELATIONS IN THE SYSTEM Fe_2O_3 - FeO - $YFeO_3$ IN AIR

FIGURE 1

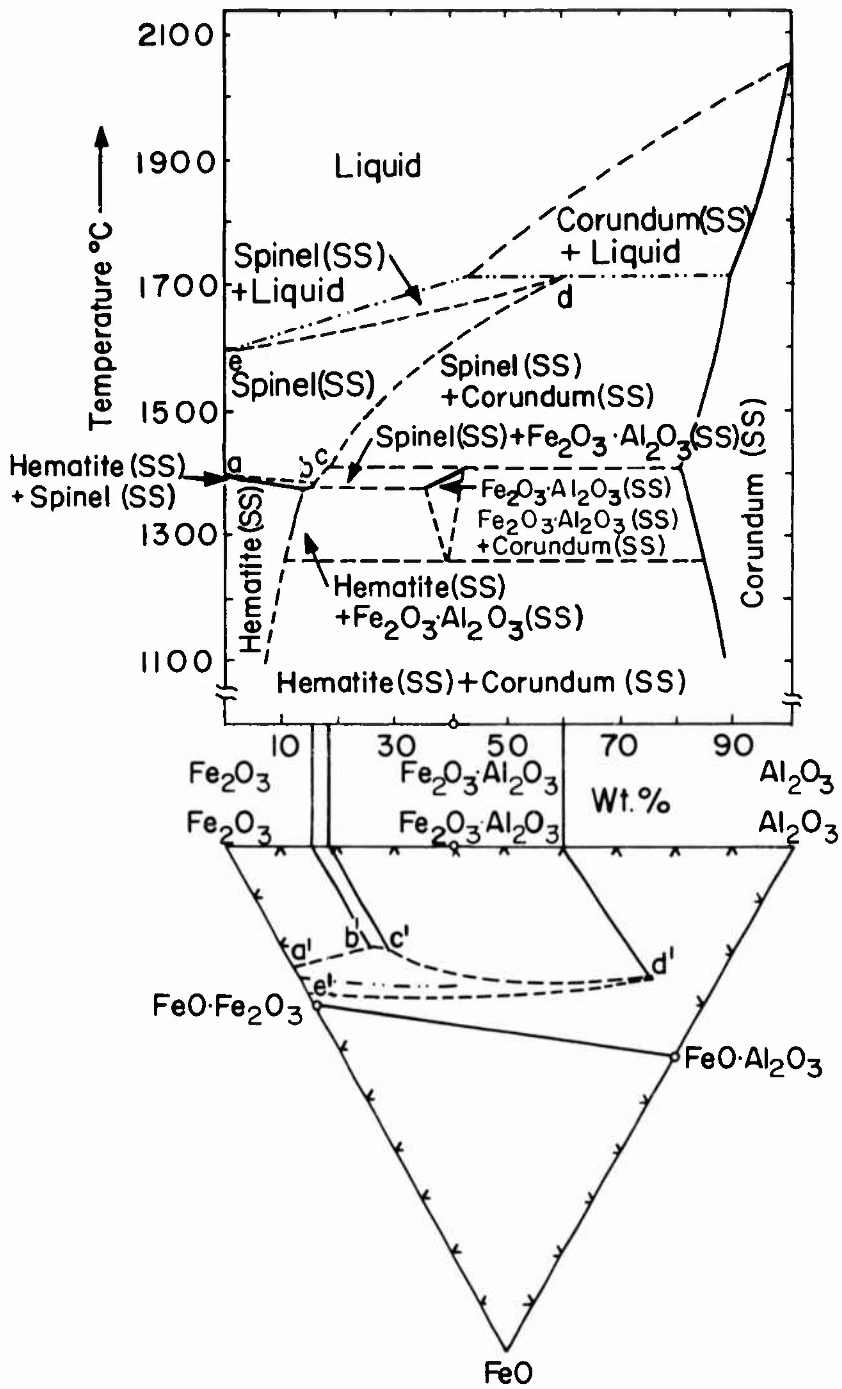

THE SYSTEM IRON OXIDE-Al_2O_3 IN AIR

(After Muan and Gee)

FIGURE 2

The data in the literature on crystalline phases and their solid solutions in the quaternary system Y-Fe-Al-O are summarized graphically in Fig. 3. The solubility relations in the Y-Gd-Fe-O system are included for comparison. The solid solutions shown as cross-tracked lines are maximum values for the various phases in an air atmosphere rather than limits for any one specific temperature. Compositions are indicated as the sesquioxides and do not show the oxygen losses which have taken place at elevated temperatures.

In the limiting systems of yttria with either alumina or iron oxide, crystalline compounds of definite proportion are formed with little or no solid solubility in excess of stoichiometry. In the iron oxide-alumina system, however, solid solution is extensive in hematite, corundum, and especially in the spinel phase. The solubility also extends into the quaternary system Y-Al-Fe-O in the garnet ($Y_3(Fe\,Al)_5O_{12}$) and orthoferrite ($Y(Al\,Fe)O_3$) crystalline phases. Solid solutions in this system arise through substitution between iron and aluminum and are therefore parallel to the Fe_2O_3-Al_2O_3 sideline; in the system Y-Gd-Fe-O the solid solutions form by substitution between yttrium and gadolinium and parallel to the Y_2O_3-Gd_2O_3 sideline.

3. Experimental Methods

Starting materials were prepared either by milling a mixture of the oxides Fe_2O_3, Al_2O_3, and Y_2O_3 or by co-precipitation of the nitrates of the same elements as hydroxides by adding the nitrate solution drop-wise to a strongly ammonical solution. The ternary composition of the materials prepared in this study are indicated in Fig. 4. Samples were calcined at 1100°C, ground, and then refired to 1300°-1400°C to further homogenize the material. Aliquots of these samples were packed in platinum vials and fired at 1400°C to 1625°C in a platinum-rhodium resistance furnace, or within an alumina muffle inserted in a gas-oxygen fired kiln for temperatures from 1600°C to 1750°C. The high-alumina compositions required repeated firings at high temperatures to produce consistent results and phases of well defined composition. As many as three separate firings for 20 hours at 1550°C with thorough grindings between each run were carried out in certain of these high alumina compositions.

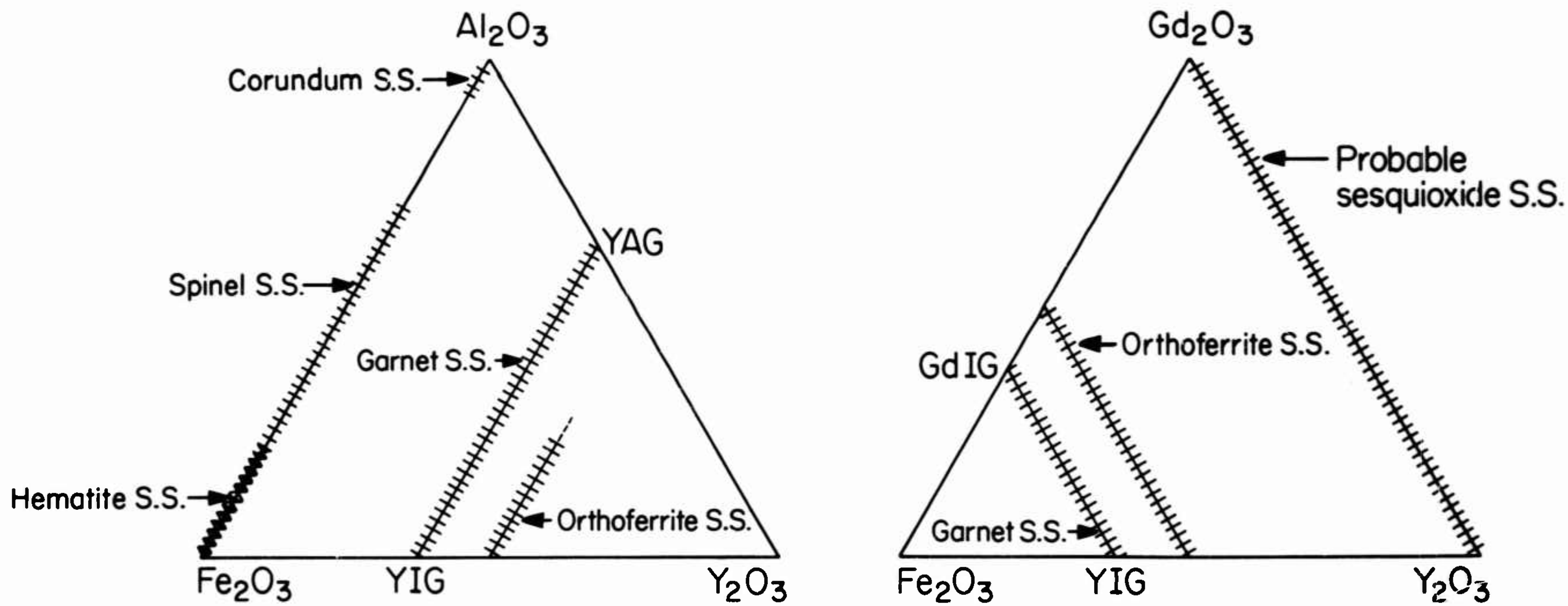

SOLUBILITY LIMITS OF CRITICAL PHASES IN SYSTEMS INVOLVING YTTRIUM IRON GARNET

FIGURE 3

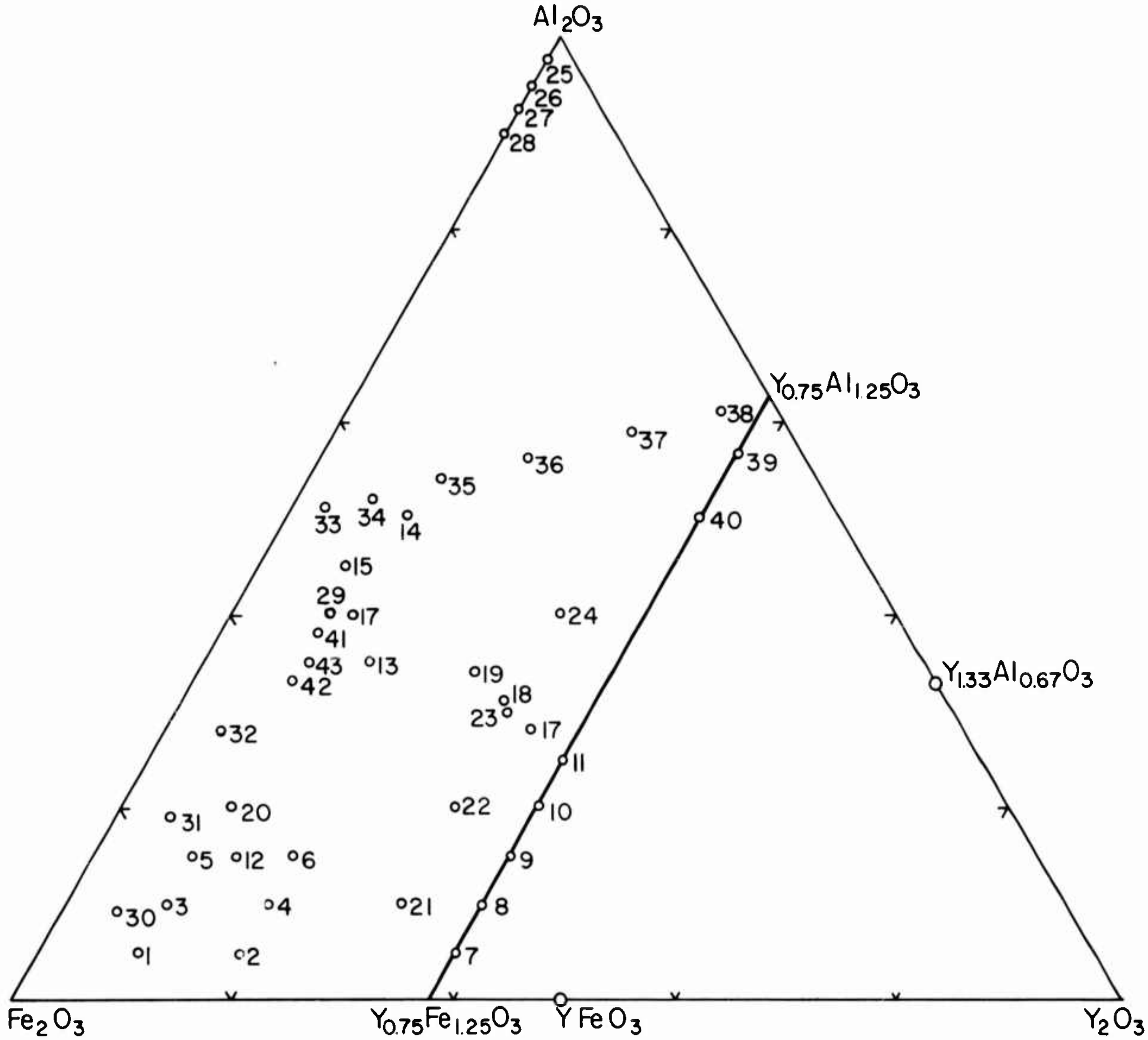

COMPOSITIONS INVESTIGATED IN THE SYSTEM Fe_2O_3–FeO–Al_2O_3–Y_2O_3

FIGURE 4

The samples were quenched in an air atmosphere for microscopic and X-ray examination. The samples intended for microscopic study as polished sections were quenched relatively slowly in stagnent air so that the liquid phase might develop the easily recognizable "eutectic" segregation structure. Samples to be examined by X-ray diffraction were quenched rapidly by dropping the sample vial directly into water at the bottom of the furnace tube. Diffraction studies were made using iron filtered cobalt radiation with slow scanning techniques (1/8° 2 θ per minute) for lattice parameter determinations.

A separate investigation was made of weight loss in air for two compositions (numbers 20 and 43, Fig. 4) in the ternary system using a Maur recording thermobalance. Weight changes were determined with an estimated accuracy of ±0. 002 gm. or approximately $x = \pm 0.005$ in $(YFeAl)_2O_{3-x}$.

4. Experimental Results

Several solid solutions are formed in the system Y-Fe-Al-O. As noted previously, solubility occurs mainly through replacement between iron and aluminum because of the size compatibility and is essentially nil between either iron or aluminum and yttrium.

Solubility is complete between YIG ($Y_3Fe_5O_{12}$) and the alumina analog YAG ($Y_3Al_5O_{12}$). The change in lattice parameter with composition is shown in Fig. 5 together with comparative data given by Geller[6] and by Maguire.[11] Some difficulty was experienced in making homogeneous samples high in alumina because of the very low reactivity of these compositions. The degree of inhomogeneity in these samples was indicated by a broadening of high angle diffraction peaks. Several firings were needed to reduce the broadening to the point that lattice parameter values could be determined within the confidence limits of ±0. 005 A; the lattice parameter of compositions near the end-member YIG could be determined with somewhat greater accuracy (±0. 002 A).

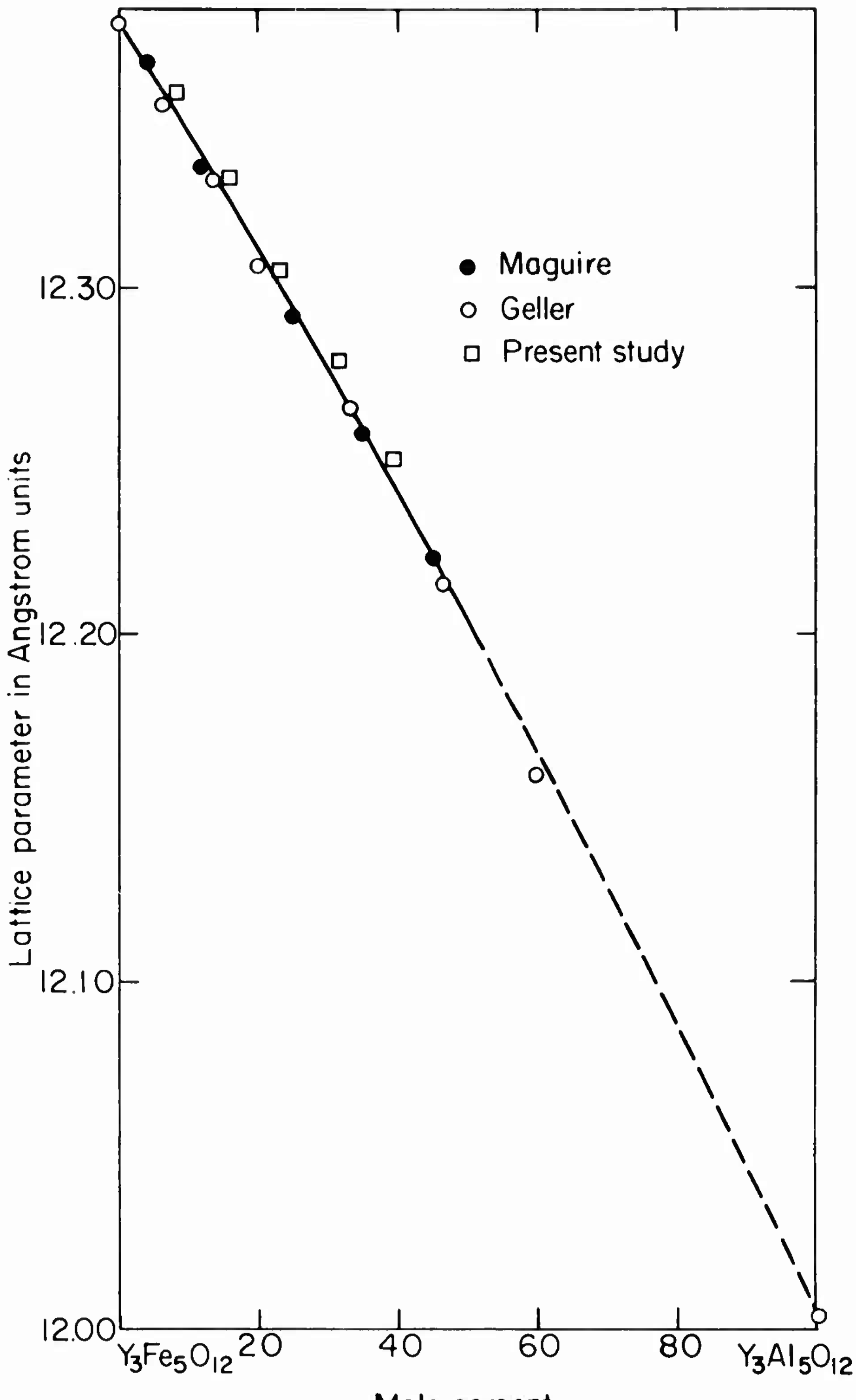

LATTICE PARAMETERS OF $Y_3Fe_5O_{12}$ – $Y_3Fe_5O_{12}$ SOLID SOLUTIONS

FIGURE 5

Solid solubility in the spinel phase has been determined by Muan and Gee[13] and by Richards and White.[14] The compositions are of the form $Fe_{3-x}Al_xO_{4+y}$ with $0 \leq x \leq 2$. A variable and undetermined amount of oxygen in excess of stoichiometry is represented as the quantity "y". Further studies on the oxygen content of these spinel compositions are reported in following sections. The results of X-ray examination are given in Fig. 6. Compositions fired in air at 1500°C have smaller lattice parameters than corresponding samples fired at 1500°C under reducing conditions apparently because of cation deficiencies in air-fired samples. No changes were noted in the lattice parameter of spinel with small amounts of yttria present compared to pure iron-alumina compositions, indicating that solubility of yttria is probably negligibly small.

The solubility of iron oxide in corundum was rather difficult to determine. A series of compositions run at 1500°C for 12 hours indicated a solubility of about 10 mole percent Fe_2O_3, but reruns of these same compositions for 24 hours at 1550°C indicated a lower solubility limit of 7 mole percent Fe_2O_3. The latter value has been taken as the equilibrium solubility. The extent of reduction of Fe_2O_3 to FeO in these high alumina samples was not determined.

Solid solutions of the type $Y(FeAl)O_3$, the orthoferrite phase, are formed in the quaternary system, extending from $YFeO_3$ towards the apparently unstable compound $YAlO_3$. The limit of the solid solution was not determined in the present study.

Phase relations in the quaternary system are shown in Fig. 7 as a ternary projection of the air isobaric section on the composition triangle Fe_2O_3-Al_2O_3-Y_2O_3. The results of critical runs used to determine the diagram are given in Table II. The basis for treating an isobar of a quaternary system of this type as a ternary projection has been discussed by Muan,[16] the essential reason is that the choice of one oxygen pressure in non-condensed systems reduces the degrees of variance by one, giving to quaternary equilibria the outward appearance of ternary relationships.

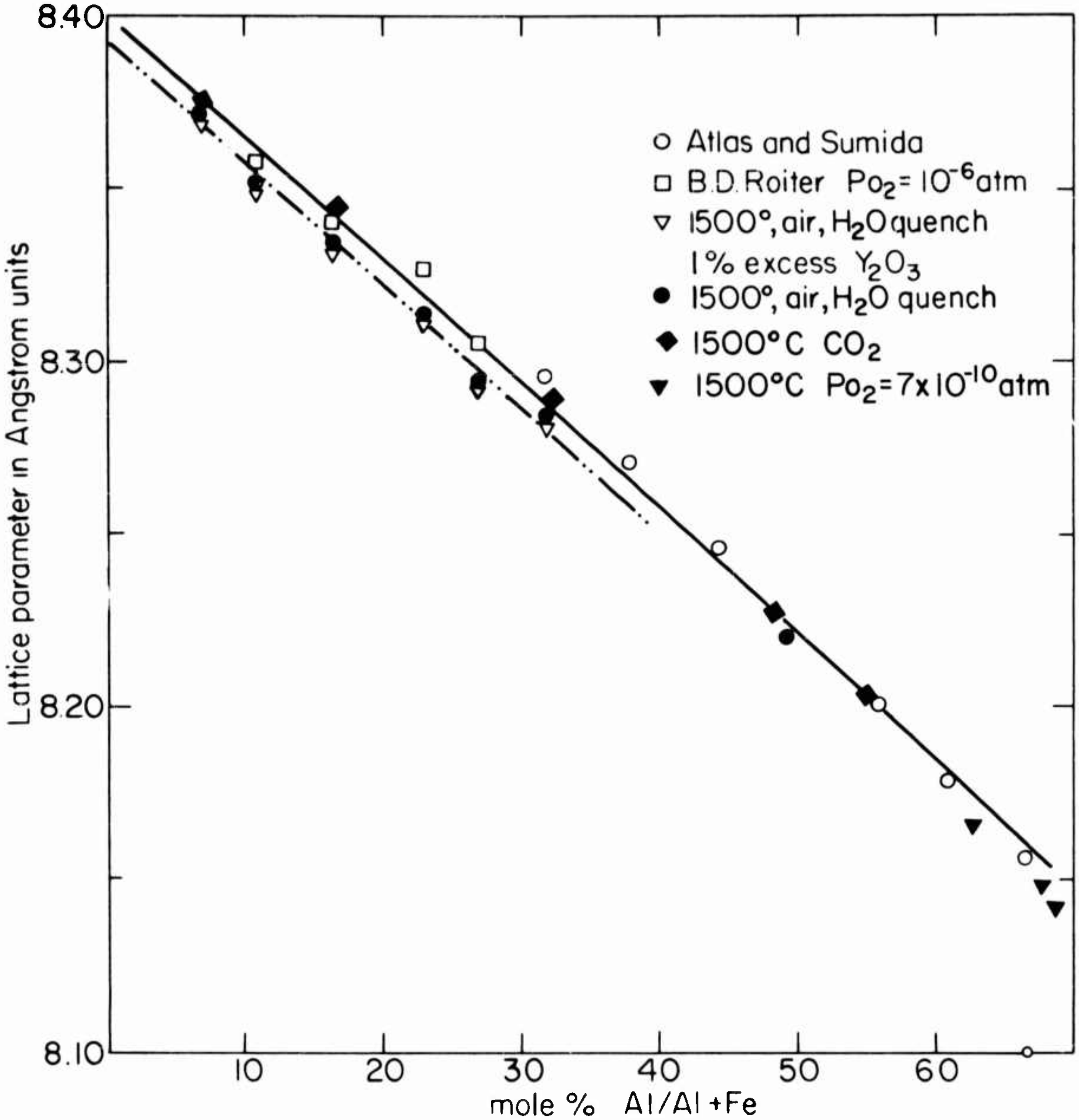

LATTICE PARAMETER OF SPINEL SOLID SOLUTIONS IN THE SYSTEM Fe-Al-O

FIGURE 6

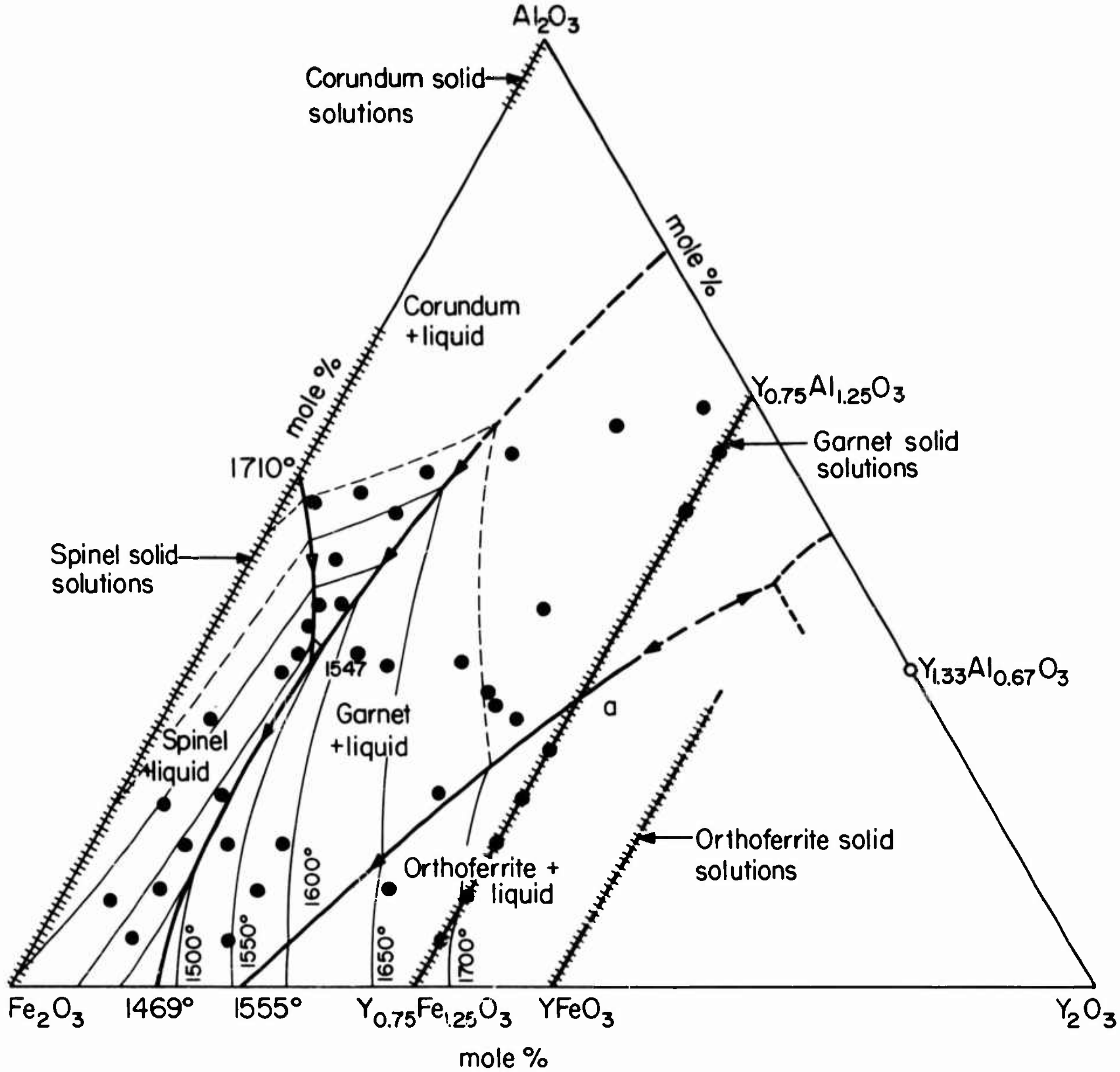

PHASE RELATIONS IN THE SYSTEM Fe_2O_3-FeO-Al_2O_3-Y_2O_3 IN AIR

FIGURE 7

TABLE II

Critical Quench Runs in the System

Fe_2O_3-Al_2O_3-Y_2O_3

Number	Composition Mole % Fe_2O_3	Al_2O_3	Y_2O_3	Temperature °C	Time in Hours	Results Lattice Parameter a_o in Angstroms
1	86	5	9	1480	16	spinel a_o = 8 36 + garnet a_o = 12 301
				1490	0.16	liquid + spinel
				1510	1.3	liquid + 2% spinel
2	77	5	18	1480	48	garnet a_o = 8.38 + spinel a_o = 12.32
				1490	1	liquid + garnet
				1520	1	liquid + garnet
3	81	10	9	1480	24	spinel a_o = 8.365 + garnet a_o = 12.278
				1490	0.16	spinel + garnet
				1500	16	liquid + spinel
				1530	1	liquid + 10% spinel
4	72	10	18	1480	48	garnet a_o = 12.295 + spinel a_o = 8.37
				1580	1	liquid + garnet
5	76	15	9	1480	24	spinel a_o = 8.346 + garnet a_o = 12.18
				1510	2	spinel + liquid
				1540	2	liquid + 20% spinel

TABLE II (Continued)

Number	Composition Mole % Fe_2O_3	Al_2O_3	Y_2O_3	Temperature °C	Time in Hours	Results Lattice Parameter a_o in Angstroms
6	67	15	18	1480	48	garnet a_o = 12.256 + spinel a_o = 8.36
				1500	1	liquid + garnet = a_o = 12.235
				1580	1	liquid + garnet
7	57.5	5	37.5	1500	16	garnet a_o = 12.356
				1580	1	garnet
				1620	0.5	orthoferrite + liquid
8	52.5	10	37.5	1500	16	garnet a_o = 12.33
				1620	0.5	garnet
				1660	0.5	orthoferrite + liquid
9	47.5	15	37.5	1500	16	garnet a_o = 12.306
				1660	0.5	garnet + orthoferrite + liquid
				1682	0.3	orthoferrite + liquid
10	42.5	20	37.5	1500	16	garnet a_o = 12.28
				1682	0.25	garnet
				1695	0.3	liquid + orthoferrite + garnet
				1710	0.16	liquid + orthoferrite + garnet
11	37.5	25	37.5	1500	16	garnet a_o = 12.25
				1670	0.3	garnet

TABLE II (Continued)

Number	Composition Mole % Fe_2O_3	Al_2O_3	Y_2O_3	Temperature °C	Time in Hours	Results Lattice Parameter a_o in Angstroms
11	37.5	25	37.5	1700	0.3	garnet + orthoferrite + liquid
				1710	0.16	garnet + orthoferrite + liquid
12	72	15	13	1515	1.5	
13	50	35	15	1520	2	garnet a_o = 12.12 + spinel
				1540	2.5	garnet + liquid
				1600	1	garnet + liquid
14	39	50	11	1540	2.5	garnet + corundum + spinel
				1550	16	garnet a_o = 12.10 + corundum + liquid
				1600	1	corundum + liquid
15	47	45	8	1540	2.5	spinel + garnet + corundum
				1570	1.5	corundum + liquid
				1600	1	corundum + liquid
16	49	40	11	1530	18	garnet + spinel
17	39	28	33	1720	0.3	garnet + liquid
				1750	0.3	liquid
18	40	31	29	1720	0.3	garnet + liquid
				1750	0.3	liquid

TABLE II (Continued)

Number	Composition Mole % Fe_2O_3	Al_2O_3	Y_2O_3	Temperature °C	Time in Hours	Results Lattice Parameter a_o in Angstroms
19	41	34	25	1720	0.3	liquid
20	70	20	10	1515	4	garnet + spinel
				1527	3	liquid + spinel quench dendrites
21	60	10	30	1500	16	garnet a_o = 12.340 + liquid
				1550	15	garnet a_o = 12.304 + liquid
				1600	4	garnet a_o = 12.295 + liquid
22	50	20	30	1500	16	garnet a_o = 12.250 + spinel
				1550	15	garnet a_o = 12.236 + liquid
				1600	4	garnet a_o = 12.228 + liquid
23	40	30	30	1550	15	garnet a_o = 12.181 + liquid
				1600	2	garnet a_o = 12.166 + liquid
24	30	40	30	1550	15	garnet a_o = 12.120 + liquid
				1600	2	garnet a_o = 12.112 + liquid
--	--	100	--	1530	48	corundum d_{214} = 1.4048 (±0.0005)
25	25	97.5	--	1530	48	corundum d_{214} = 1.4067
26	5	95	--	1530	48	corundum d_{214} = 1.4088
27	7.5	92.5	--	1530	48	corundum d_{214} = 1.4090 + spinel

TABLE II (Continued)

Number	Composition Mole % Fe_2O_3	Al_2O_3	Y_2O_3	Temperature °C	Time in Hours	Results Lattice Parameter a_o in Angstroms
28	10	90	--	1530	48	corundum d_{214} = 1.4094 + spinel
29	51	40	9	1545	4	garnet + spinel
				1550	4	corundum + spinel + liquid
30	86	9	5	1550	17	spinel a_o = 8.355 + liquid
31	76	19	5	1550	17	spinel a_o = 8.32 + liquid
32	67	28	5	1550	17	spinel a_o = 8.28 + liquid
33	46	51	3	1550	37.5	spinel a_o = 8.21 + corundum d_{214} = 1.410 + liquid
34	41	52	7	1550	32	liquid (?) + corundum d_{214} = 1.410
35	34	54	12	1550	32	garnet a_o = 12.093 + corundum d_{214} = 1.415 + liquid
36	25	56	19	1550	37.5	garnet a_o = 12.091 + corundum d_{214} = 1.414 + liquid
37	14	59	27	1550	32	garnet a_o = 12.087 + corundum d_{214} = 1.416
38	5	61	34	1550	37.5	garnet a_o = 12.035 + corundum
39	6	56.5	37.5	1750	0.6	garnet
40	12.5	50	37.5	1750	0.6	garnet

TABLE II (Continued)

Number	Composition Mole % Fe_2O_3	Al_2O_3	Y_2O_3	Temperature °C	Time in Hours	Results Lattice Parameter a_o in Angstroms
41	53	38	9	1550	1	spinel + corundum + liquid
42	58	32	9	1550	1	liquid + spinel quench phase
43	55.5	35	9.5	1550	1	liquid + spinel quench phase + trace corundum

Melting temperatures in the ternary air isobar vary from 1469°C, the eutectic temperature in the Y-Fe-O system to approximately 2050°C, the melting point of pure Al_2O_3. The isobaric eutectic between spinel and garnet in the Y-Fe-O system (Fig. 1) is extended into the ternary diagram as the boundary curve separating the primary crystallization fields of alumina-bearing spinel and garnet solid solutions. The boundary curve terminates at the isobaric ternary peritectic where the fields of corundum, spinel, and garnet intersect. This point is invariant in air occurring at 1547°±5°C at a liquid composition $Y_{0.22}Al_{0.70}Fe_{1.08}O_{2.835}$. The three solid solutions at equilibrium with the above oxide liquid are garnet $Y_{0.75}Al_{0.94}Fe_{0.31}O_3$, spinel $Fe_{1.74}Al_{1.16}O_4$ and corundum $Al_{1.86}Fe_{0.14}O_3$. Between 1547°C and 1469°C garnet solid solutions in the composition range $Y_3Al_{3.8}Fe_{1.2}O_{12}$ to $Y_3Fe_5O_{12}$ can coexist with oxide liquid.

The compound YIG melts incongruently to iron oxide rich liquid and a second orthoferrite phase in the system Y-Fe-O. This incongruent melting is extended into the quaternary system for garnet compositions below the intersection of the garnet join with the boundary curve for coexisting garnet, orthoferrite and oxide liquid (point a, Fig. 7). For garnet compositions from $Y_3Fe_5O_{12}$ to $Y_3Al_{2.4}Fe_{2.6}O_{12}$, the orthoferrite plus liquid crystallization field is intersected before the temperature of complete melting is reached. This is shown in Fig. 8 which is a composition plane through the air isobar at the join between $Y_3Fe_5O_{12}$ and $Y_3Al_5O_{12}$. The composition of the orthoferrite and oxide liquid phases (light lines) are displaced from the plane of section and in these areas the join is not binary. The portions of the join that are binary for the air isobar, i. e., where composition can be stated as proportions of $Y_3Fe_5O_{12}$ and $Y_3Al_5O_{12}$ are shown in heavy lines. As in the previous figures, the dashed lines indicate inferred relationships not determined experimentally.

The solid solutions which arise in the system contribute an added variable to the study of phase relations at melting temperatures since the composition of the solid phase or phases as well as that of the liquid oxide can vary within wide limits. The situation has been simplified throughout this discussion by

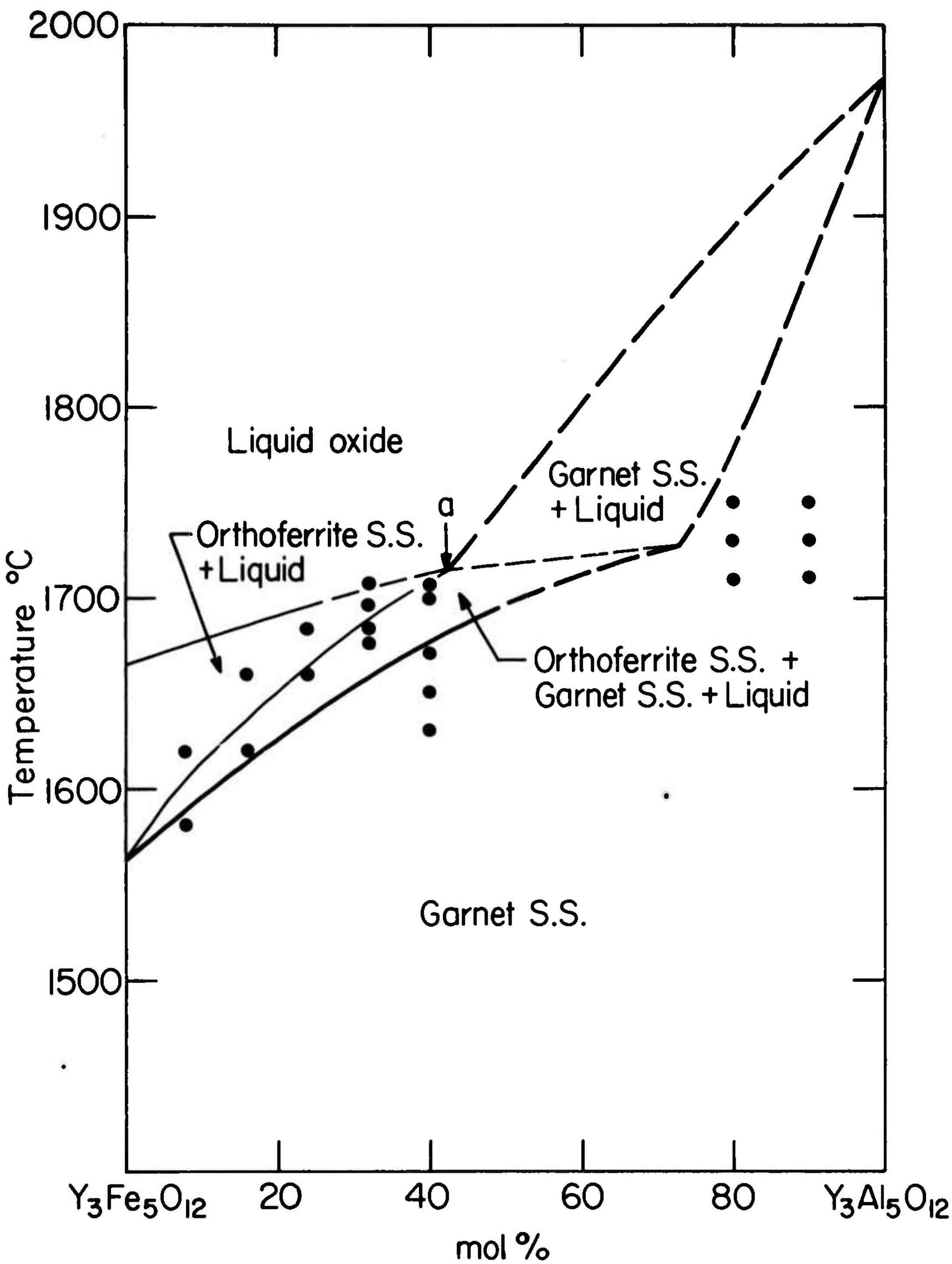

A SECTION THROUGH THE AIR ISOBAR OF THE SYSTEM Y-Al-Fe-O ON THE JOIN $Y_3Fe_5O_{12}$ - $Y_3Al_5O_{12}$

FIGURE 8

the assignment of a fixed oxygen partial pressure and by neglecting the changes in oxygen fraction with temperature and starting composition. A further simplification can be made by choosing one temperature and constructing an isothermal-isobaric section through the system; the only remaining variable is starting composition which can be represented in terms of three components by a ternary diagram. This has been done for the 1550°C isotherm which was investigated in some detail to clarify the phase relations and to provide data for later crystal growth experiments. In Fig. 9 phase relations are shown in the air isobar - 1550°C isotherm. Liquid oxide is found over a composition range which narrows with increasing aluminum content, extending to a composition in the vicinity of the air isobar peritectic point. In the two-phase regions, tie lines are drawn between coexisting phases. Note that in both the region of garnet plus liquid and spinel plus liquid, the crystalline phase is considerably higher in alumina content than the liquid phase. Two three-phase areas have been determined at high alumina compositions, the first comprising spinel $Fe_{1.7}Al_{1.2}O_4$ (a) plus corundum $Al_{1.80}Fe_{0.20}O_3$ (d) plus liquid $Y_{0.22}Fe_{1.04}Al_{0.74}O_{2.83}$ (b) the second, corundum $Al_{1.80}Fe_{0.20}O_3$ (d) plus garnet $Y_{0.75}Fe_{0.31}Al_{0.94}O_3$ (e) plus liquid $Y_{0.24}Fe_{1.02}Al_{0.74}O_{2.83}$ (c).

At temperatures above 1550°C, isothermal-isobaric sections are characterized by a progressive widening of the region of oxide liquid into spinel and garnet crystallization fields. The rapid increase of liquidus temperatures in the corundum field limits the extension of oxide liquid to higher alumina content until very high temperatures are attained. At temperatures below 1550°C, the oxide liquid region narrows and contracts following the garnet plus spinel plus liquid boundary curve as shown by the trend of liquid isotherms in Fig. 7. Below 1469°C in air, there is stable oxide liquid present.

5. Discussion

The primary crystallization field of garnet (Fig. 7) covers a wide range of starting compositions. The field widens rapidly as alumina is added to yttria-iron oxide mixtures due in particular to the trend of the boundary curve

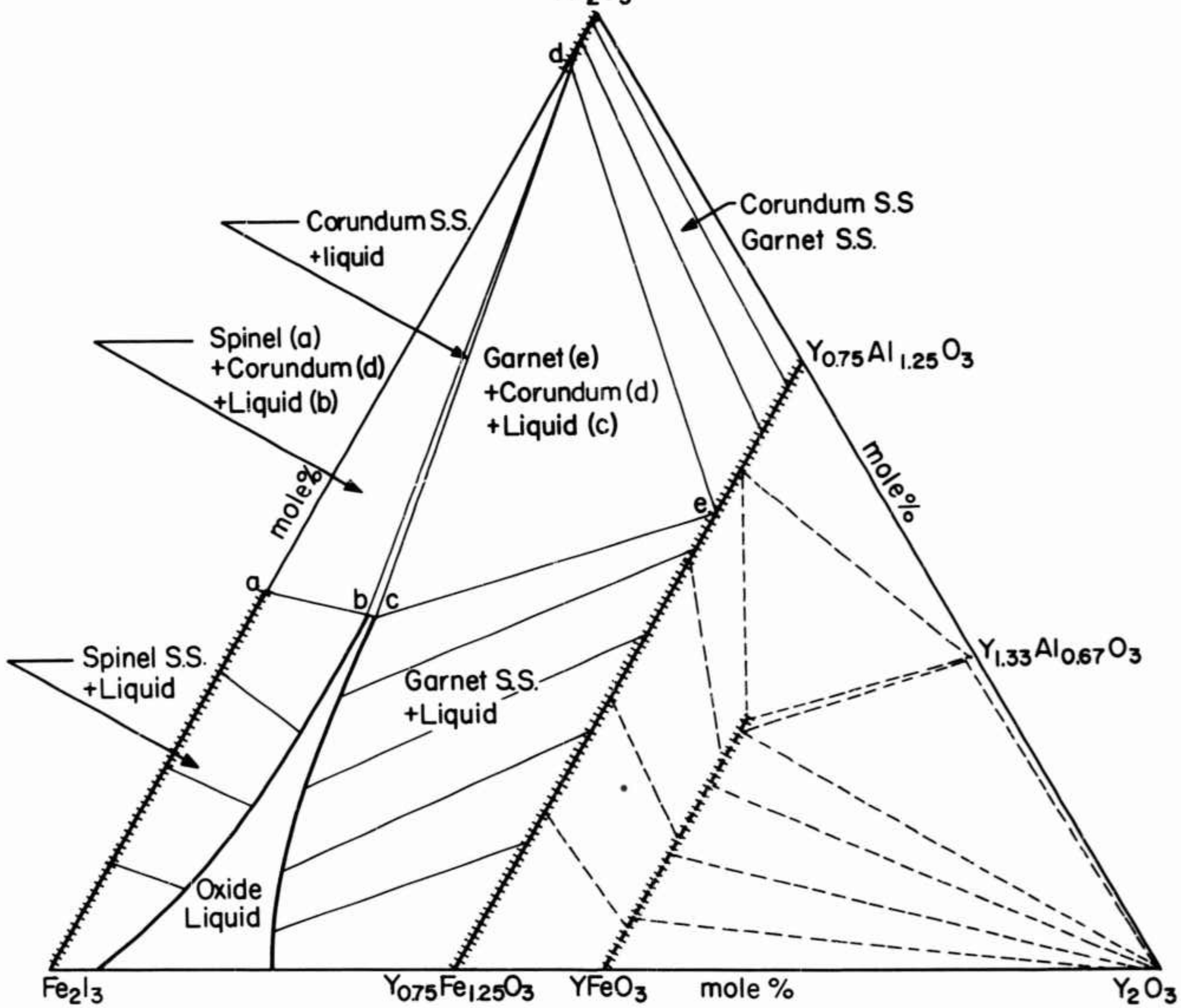

PHASE EQUILIBRIA FOR THE AIR ISOBARIC-1550°C ISOTHERMAL SECTION OF THE SYSTEM Y-Fe-Al-O

FIGURE 9

separating the primary fields of garnet and orthoferrite solid solutions. At compositions above $Y_3Fe_{2.6}Al_{2.4}O_{12}$ at 1715°C (point a, Fig. 7), garnet can be crystallized from liquids with a higher yttria content than that of the separating garnet phase. Between this garnet composition and pure YIG, melting is incongruent with the intrusion of the orthoferrite phase at liquidus temperatures. The point at which the boundary curve crosses the $Y_3Fe_5O_{12}$ - $Y_3Al_5O_{12}$ join is also shown by the composition join Fig. 8. In Fig. 8 a relatively narrow range of coexisting garnet, orthoferrite, and liquid can be seen separating single phase garnet and oxide melt regions. In crystal growth in which there exists a very sharp temperature drop at the growth in surface, for example in the Verneuil method, it may be possible to "bridge" the three-phase region in which segregation occurs and effectively grow crystals from a quasi-homogeneous liquid as if congruent melting were the case.[17]

In general however, the garnets with higher iron content in the range $Y_3Fe_{5-x}Al_xO_{12}$ wher $0 \geq x \geq 1$ have more interesting magnetic properties[11] and are more desirable as single crystals. For these compositions melting is incongruent as is the case for pure YIG and crystal growth will necessarily take place from liquids near the boundary curve separating garnet and spinel crystallization surfaces (Fig. 7), i. e., from melts enriched in iron oxide. Paths of equilibrium crystallization in this region are complicated somewhat by continuous changes in composition of coexisting solid solution and oxide liquid with decreasing temperature. The garnet or spinel solid solution separating out at the higher temperatures has a larger Al:Fe ratio, and as the temperature decreases, interaction of liquid and solid produces a homogeneous phase progressively higher in iron content assuming equilibrium is maintained. If equilibrium is not maintained, i. e., if diffusion and homogenization do not keep up with the rate of temperature decrease, the crystal will be zoned with higher Al:Fe ratio in the core and outer layers approaching pure YIG in composition.

Turning first to equilibrium crystal growth, consider the crystallization of composition w in Fig. 10 which is on the boundary curve separating crystallization fields of garnet and spinel solid solutions. For this sample crystallization

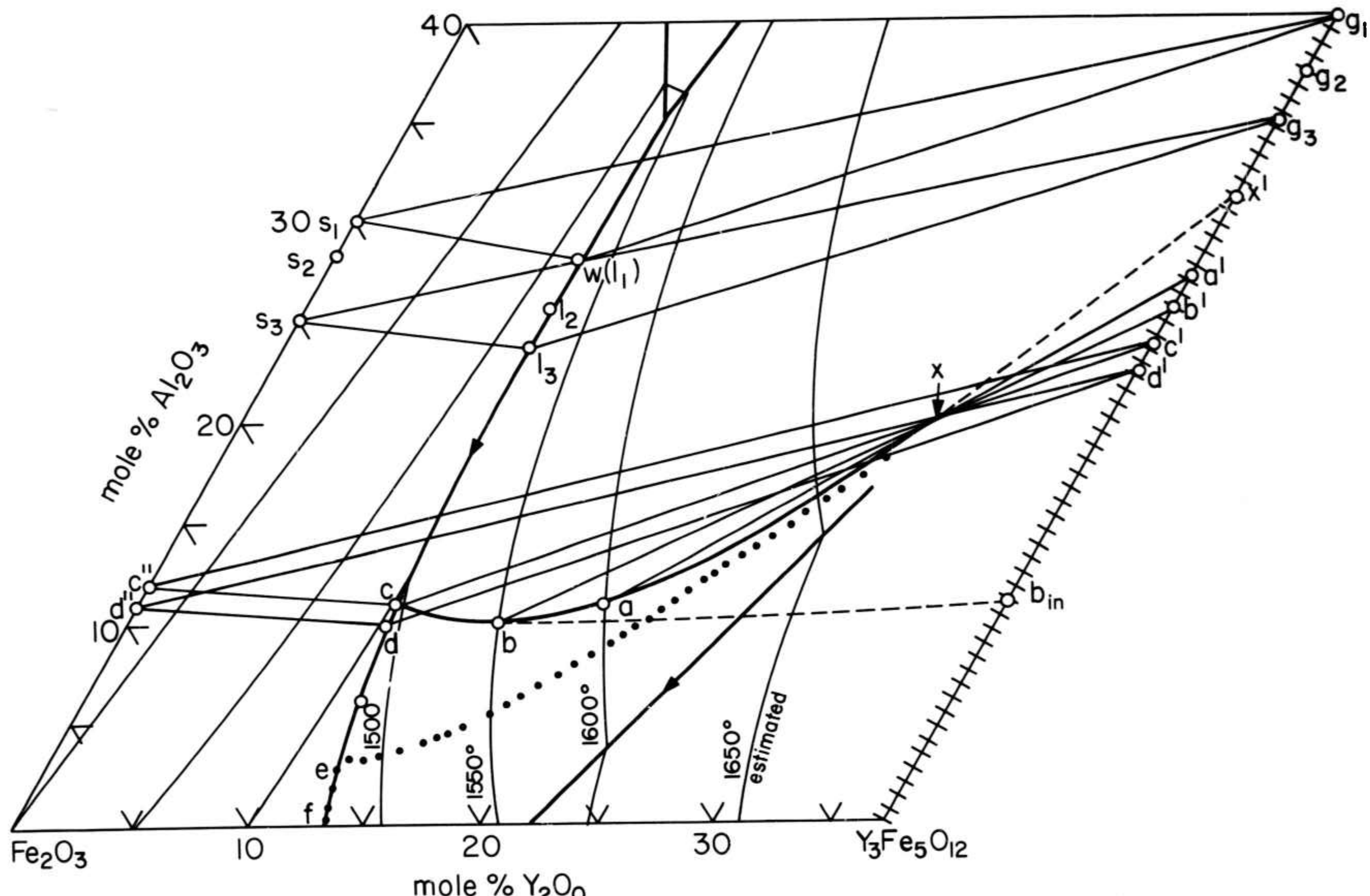

EQUILIBRIUM CRYSTALLIZATION PATHS IN THE SYSTEM $Fe_2O_3-FeO-Al_2O_3-Y_2O_3$

FIGURE 10

begins at 1536°C with spinel s_1 and garnet g_1 separating out simultaneously. At some intermediate temperature the system will consist of spinel s_2 and ℓ_2 and garnet g_2 with total composition w within the composition triangle. At 1529°C crystallization is completed as the last trace of liquid, now at ℓ_3 disappears leaving spinel s_3 and garnet g_3.

However, in crystal growth one is concerned with producing a single homogeneous phase rather than a co-precipitated mixture of two phases as is the case of composition w. For this reason, crystal growth must terminate before the liquid composition intersects the boundary curve and the second phase begins to separate out. The point of intersection with the boundary curve is indicated in temperature and composition by three phase triangles representing coexisting spinel, garnet, and liquid phases. Data are given for a number of these three phase triangles in Table III.

In the two-phase regions where liquid and only one solid phase coexist, the paths of crystallization are more complex than in the case previously described involving two solids and a liquid. During crystallization the liquid composition follows a curved path until the ternary isobaric boundary curve is intersected. The path of crystallization is different for each starting composition and depends on the disposition of ternary fractionation curve at each point. The general form of the crystallization path is, however, the same in these regions and one example should suffice to show the trend.

Consider the equilibrium crystallization of a total composition 50% Fe_2O_3, 20% Al_2O_3, 30% Y_2O_3 (composition 22, TableII) indicated as point x in Fig. 10. Crystal growth begins at some temperature above 1650°C, the first garnet separating having composition x'. At 1600°C the liquid composition has moved from x to a. The garnet has changed similarly from x' to a' through a continuous reaction with oxide liquid. The "instantaneous" composition of garnet separating out is given by the tangent to crystallization curve at each temperature. The resulting iron-rich garnet outer layer (garnet composition $b_{\text{"in"}}$ separating instantaneously at 1550°C) reacts with the bulk of the solid to produce a total composition slightly higher in iron (moving from

TABLE III

Composition of Condensed Phases in Air Along the Garnet + Spinel + Liquid Boundary Curve

Temp.	Garnet	Composition Spinel	Oxide Liquid
1469°C	$Y_{0.75}Fe_{1.25}O_3$	$Fe_{2.94}O_4^*$	$Y_{0.27}Fe_{1.27}O_{2.87}$
1484°C	$Y_{0.75}Fe_{1.04}Al_{0.21}O_3$	$Fe_{2.80}Al_{0.13}O_4$	$Y_{0.24}Fe_{1.66}Al_{0.10}O_{2.85}$
1503°C	$Y_{0.75}Fe_{0.81}Al_{0.45}O_3$	$Fe_{2.57}Al_{0.35}O_4$	$Y_{0.22}Fe_{1.54}Al_{0.24}O_{2.83}$
1521°C	$Y_{0.75}Fe_{0.60}Al_{0.65}O_3$	$Fe_{2.31}Al_{0.61}O_4$	$Y_{0.22}Fe_{1.38}Al_{0.41}O_{2.83}$
1540°C	$Y_{0.75}Fe_{0.42}Al_{0.84}O_3$	$Fe_{1.99}Al_{0.91}O_4$	$Y_{0.21}Fe_{1.20}Al_{0.59}O_{2.83}$
1547°C	$Y_{0.75}Fe_{0.32}Al_{0.94}O_3$	$Fe_{1.74}Al_{1.16}O_4$	$Y_{0.22}Fe_{1.08}Al_{0.20}O_{2.83}$

*Oxygen fraction of the spinel phase estimated from data given by Richards and White.[14]

$b_{''in''}$ towards c'). The process continues with decreasing temperature, total composition x consisting of liquid b and garnet b' at 1550°C and liquid c and garnet c' at 1495°C. At 1495°C the system contains 72% garnet c' (distance c x ÷ distance c c') and 28% liquid c. At this point the liquid has been enriched in iron oxide to the degree that a spinel phase of composition c'' begins to separate out. Crystallization is completed at a slightly lower temperature where garnet d', spinel d'' and the last trace of liquid, now at composition d, coexist. During the process the garnet has changed from x' to d' and the liquid from x to d.

Similar compositional variations can be found for all garnets crystallizing at equilibrium from iron oxide rich liquids. The changes in composition are more pronounced for high alumina mixtures and decrease as total composition approaches the iron oxide-yttrium oxide join.

Non-equilibrium crystallization will arise in all cases where reaction between the solid phase and oxide liquid is incomplete. The liquid phase must be in equilibrium with the entire bulk of the solid phase rather than just the exterior layers. This implies a relatively rapid diffusion through the crystal to continuously homogenize the phase as the growing conditions change. Considering the stringent requirement of continuous compositional changes in adjusting to equilibrium at each temperature during growth, it is not surprising that non-equilibrium or fractional crystallization does often occur.

In the growth of garnet solid solutions from the melt, the end result of perfect fractional crystallization in every case would be alumina enriched crystals and a residual liquid $Y_{0.27}Fe_{1.73}O_{2.87}$ corresponding to the air isobar eutectic in the Y-Fe-O system. The outermost layer crystallized from this liquid would then be pure yttrium iron garnet (YIG) and iron spinel (Fe_3O_3). The path of fractional crystallization of composition x (Fig. 10) would follow approximately the dotted x-e-f which falls below the equilibrium crystallization path x-a-b-c-d. The crystal resulting from growth along the x-e-f would have a core of garnet composition x' and an exterior of almost pure YIG interspersed with a second spinel phase, nominally Fe_3O_4.

Such relatively abrupt composition changes or zoning effects are undesirable in single crystals for several reasons. Large compositional changes may cause sufficient misfit in lattice dimensions to introduce considerable strain. This condition would have a disrupting effect on crystal growth and might result in degeneration to polycrystal growth. Furthermore, the non-homogeneity would probably be very difficult to remove by annealing in garnet crystals because of the very unreactive nature of the material. This has been shown by the difficulty in obtaining samples of homogeneous composition for X-ray study.

The phase relations for the air isobar in the quaternary system Y-Fe-Al-O can be extended to other oxygen atmospheres based on knowledge of the system Y-Fe-O[12] which has also been studied in oxygen (P_{O_2} = 760 mm Hg) and CO_2 (P_{O_2} variable) atmospheres. Higher oxygen pressure extends the crystallization field of the garnet by suppressing its decomposition until higher temperatures. Low oxygen pressure environments have the opposite effect of narrowing the field of garnet plus liquid by promoting decomposition of garnet at low temperatures. In the quaternary system, one might expect a similar dependence of the garnet plus liquid crystallization surface on oxygen partial pressure. Since the effect of oxygen pressure on melting relations is due largely to the ferrous-ferric ratio, the changes are expected to be most noticeable near the Fe_2O_3-Y_2O_3 sideline. Addition of the stable oxide Al_2O_3 probably dilutes the effect of oxygen pressure on melting relations to the extent that very little effect can be seen at higher alumina content.

D. Crystal Growing

1. Implications of the Phase Equilibrium Studies

From the results of the phase equilibrium studies it is possible to list several factors which are likely to have important effects on the growth of magnetic garnet single crystals. One such factor is the incongruent melting of YIG and related substituted garnets. Crystallization can only occur at

temperatures below the decomposition point and above the minimum melting temperature, and from oxide liquids whose composition at each temperature is indicated by the intersection with the ternary liquids surface. Of the magnetic garnet compositions studied thus far, all have shown a relatively small temperature range for the coexistence of garnet and liquid phases. This range in temperature can be increased by increasing the ambient oxygen pressure or decreased by a corresponding pressure decrease; for most compositions the interval is approximately 100°C, generally occurring between 1500°C and 1600°C.

Higher growth temperatures require higher oxygen pressures to suppress the decomposition of the garnet phase, but do not change very significantly the solubility of yttria (and therefore YIG) in the oxide liquid. At 10 atmospheres oxygen pressure the estimated decomposition of peritectic temperature is 1625°C and the solubility of Y_2O_3 in the oxide melt is approximately 25 mole percent as estimated from the trend of the ternary boundary curve. This liquid composition is considerably different from the liquid solubility corresponding to congruent melting of the compound, i. e., 37.5 mole percent Y_2O_3. If extrapolation of the data to higher oxygen pressures had suggested congruent melting or a reasonably close approach to congruence in liquid composition through a change in direction of the boundary curve, then crystal growth under high oxygen pressure would have been desirable. This is because congruently melting solids are generally easier to grow as single crystals since the process involves no composition changes being primarily one of a rearrangement at atoms at the interface from disordered liquid to ordered crystalline solid. This applies with equal weight to all techniques of growth from the melt, i.e., Verneuil, Bridgman, zone melting, or Czochralski. Crystal growth of incongruently melting solids is possible by any of the above methods, but is more difficult because it requires transport of solute through a concentration gradient and a more complex sequence of incorporation of solute material and rejection of solvent at the growth interface.

From considerations of solubility changes with temperature as derived from the phase diagram, it is evident that very precise temperature control during growth is desirable. For a crystal 1 cm in diameter growing at

4 mm/hr., the amount crystallized per hour is 1.6 gm. For a batch weighing 200 gm of starting composition 25 mole % Y_2O_3, 75 mole % Fe_2O_3, this amount crystallized corresponds to a drop in temperature of about 2°C/hr. Temperature control of the system as a whole must be better than 2°C to allow the temperature drop of this magnitude to occur gradually over one hour. With proper instrumentation, temperature can be maintained within these limits especially using growth techniques where a fairly large mass of material is involved as in Bridgman-Stockbarger, or Czochralski where the smaller fluctuations in temperature are avoided.

One other factor that is very important in the crystal growth of incongruently melting compounds is the creation of a sharp temperature gradient at the interface between liquid and crystallizing solid to avoid what has been described as "constitutional supercooling."[18] The phenomenon arises when the actual temperature gradient in the liquid proceeding from the interface is less than an imaginary temperature gradient determined by the change in solute concentration with distance from the interface and corresponding to the equilibrium diagram liquidus curve. When this occurs, the liquid at some point in advance of the interface has a greater supersaturation than at the interface and this induces faster growth for any area of solid momentarily in advance of the planar interface. The result is a breakdown of the stable planar interface to a "cellular" structure and the inclusion of quench phase between dendritic spikes of solid phase; in short a complete disruption of orderly growth. To avoid this condition, the temperature gradient at or near the true interface must be maximized. The high temperature gradient also increases transport of solute to the interface thereby accelerating the growth rate. The temperature gradient can become excessive and create other problems. Crystals grown by the Verneuil and zone melting methods for example, have a tendency to fracture because almost all of the heating is concentrated in a small volume of liquid leaving enormous gradients in the solid. The temperature gradients that are responsible for this rapid growth also cause thermal stresses in the material and a compromise must be sought between growth rate and crystal perfection.

2. Various Methods of Crystal Growth

The various techniques either proposed or now in use for growing the magnetic garnets are shown diagramatically in Fig. 11. The Verneuil technique has been successfully applied to growing YIG single crystals as reported by Rudness and Kebler.[3] In this method, a powder of YIG composition is liquified by falling through a high temperature zone and onto a molten pool of iron oxide rich liquid. It is not certain whether the droplets are entirely liquid or a mixture of orthoferrite crystallites plus liquid, but there is obviously very little chance for any major segregation. As the droplets fall in the molten cap of the boule, a corresponding amount of YIG crystallizes at some distance below the surface. One advantage of the process is that growth can be maintained continuously until the powder is entirely consumed. Also, no crucible is necessary to contain the material. Because of the extreme temperature gradient, growth rates are maximized by this process. Although the high temperature gradients contribute to high growth rates, they also generate internal stresses in the crystals which are difficult to remove by annealing and may cause the boule to shatter. The reducing conditions normally found in the flame fusion technique, which are undesirable for YIG growth, can be avoided by using induction heating[4] and high temperature plasmas.[19] One disadvantage in Verneuil growth is the tendency for overflow of the melt due to the very high fluidity of the oxide liquid.

The floating zone method[5] is essentially a variation of the Verneuil technique where a solid polycrystalline rod replaces the powder falling onto the melt surface. This process is also continuous and requires no containing crucible. A small zone of iron oxide enriched liquid is passed along a polycrystalline rod melting polycrystalline material and depositing single crystalline YIG behind the advancing zone. As in the related Verneuil technique, the problems of "spill out," loss of zone, bubbling of the liquid zone require constant monitoring during growth. The small mass of the high temperature liquid zone poses the additional problem of controlling temperature fluctuations during growth, but does make it easier to pressurize the system during growth.

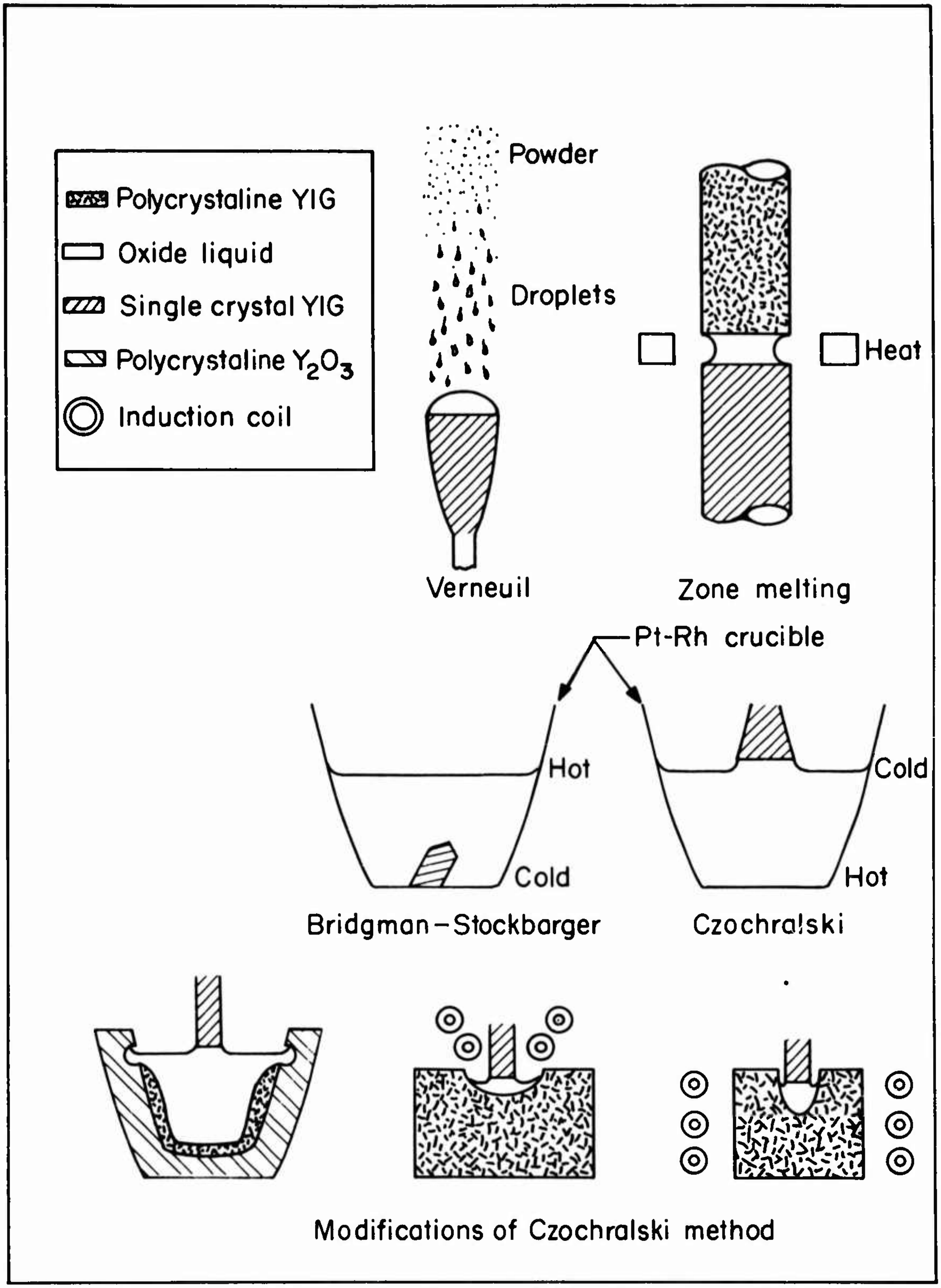

CRYSTAL GROWING METHODS APPLIED TO YTTRIUM IRON GARNET

FIGURE 11

The Bridgman-Stockbarger and Czochralski techniques[20] generally involve greater mass of liquid and are therefore less susceptible to temperature fluctuations. The process is generally not continuous, as it is in the above methods. Usually the temperature is raised high enough to liquify the entire mass and crystallization takes place through slow cooling and stops before the freezing point or "eutectic" temperature is reached. In crystal growth of YIG in air, the maximum yield of crystallized garnet by this method would be approximately 40 wt. % of the total mass of starting material, which is certainly sufficient to yield large enough single crystals. Crystallization takes place at the surface of the melt in the Czochralski technique and below the surface using the Bridgman-Stockbarger method. The Czochralski technique holds some advantage over Bridgman-Stockbarger growth in that nucleation and growth can be confined to one site, that is, at the liquid surface on the pulling rod. Also, the pulled crystal can be easily lifted from the liquid surface after the run and the melt can be replenished with material for the next pulling experiment. Using the Bridgman-Stockbarger technique, the crystals can only be recovered by slowly dissolving the melt with concentrated solvents or by destroying the crucible and cutting out the crystals. With Czochralski growth it is also possible to control the size and shape of the crystal by changes in the pulling rate. Crystals are also free of mechanical strains and have a smaller proportion of thermal stresses because of the annealing which takes place above the surface of the relatively large liquid mass. The major disadvantage in Czochralski and Bridgman-Stockbarger growth lies in the contamination of melt and crystal by the crucible material.

Several schemes have been suggested to avoid the contamination of oxide liquid by the crucible during Czochralski growth. One method[1] is to make the containing crucible out of yttrium oxide so that the corrosion of the container provides the supersaturation necessary for continued growth. Using this technique, five moles of iron oxide are removed from the liquid for every three moles of yttria dissolved from the containing crucible so that the amount of liquid does decrease during growth.

Another technique which has been used successfully is Czochralski growth using polycrystalline material of the same composition as the desired single crystal product. Two different variations have been described, one by Lepore, Wenkus, and Nielsen[21] and one by Monforte, Swanekamp, and Van Uitert.[22] In the Lepore method, an rf coil is placed above a block of polycrystalline material selectively melting a portion of the block, generally by first melting magnetite or some other lossy material on the surface. If thermal fracture can be avoided and the oxide melt kept from spreading too rapidly through increased coupling with temperature, a stable pool of liquid can be developed from which a single crystal can be extracted. The variation of this method utilized by Monforte et al. involves the positioning of the water cooled induction coil (see Fig. 11) which in his system is placed around a polycrystalline block of material. The rf energy is concentrated in the central region liquifying some of the material, whereas the outside surface of the block is kept cool by thermal contact with the induction coil. A major problem with this technique is again avoiding fracture of the polycrystalline block which is continuously water cooled on the outside and contains oxide liquid at approximately 1600°C in the center. It seems likely that crystals grown by this technique would have approximately the same thermal stress as crystals produced by the Verneuil or floating zone methods.

After considering the relative merits of the various techniques outlined above, it was decided that the method most likely to yield sound single crystals with a minimum of internal strains and imperfections would be the Czochralski technique using a platinum crucible to contain a melt of about 150 g. The crystals were to be grown in an air atmosphere and subsequently annealed in different oxygen atmospheres to evaluate this effect on their properties. Further measurements would be made to determine the concentration of platinum on the YIG crystals and to determine which properties were most strongly affected by this impurity.

3. Czochralski Growth of YIG

In order to reach and control at temperatures in the range of 1500°C to 1600°C in an oxidizing atmosphere, a crystal pulling furnace with $MoSi_2$

(Super-Kanthal) heating elements was constructed. Six hairpin shaped elements were placed around a three-inch diameter alumina tube, thirty inches long, which served as the reaction zone of the furnace. The ends of the alumina tube were sealed by water cooled brass units so that controlled atmospheres could be used. The pulling rod assembly was introduced into the furnace through an O-ring seal at the top. A glass sighting port was also located in the brass head at the top of the furnace. The crucible was placed on an adjustable pedestal at a height near the thermal center of the furnace. Rotation rates of 30, 60, and 120 rpm were used in conjunction with pulling rates of 0.01 and 0.20 inches per hour.

Several different crucible materials were investigated as to their relative resistance to attack by the oxide liquid. Previous experience had indicated that metals of the platinum group were the most promising materials for use in oxidizing atmospheres between 1500° - 1600°C although all are subject to some deterioration under these conditions. Of the more refractory metals that are economically feasible for use as crucible materials, platinum, rhodium, and iridium and alloys of these elements seem best suited. Of these elements iridium is the most susceptible to oxidation, but is also the most refractory (melting point 2450°C); it can be used at oxygen partial pressure up to about 10^{-2} atmosphere at 1600°C with pure CO_2 being convenient for this purpose. Since pure iridium would oxidize too rapidly for our purposes, and 80% platinum, 20% iridium alloy crucible was purchased. Upon firing in air at 1500°C, the crucible became extremely brittle and failed in a few hours, indicating that the alloy, although more refractory, was too susceptible to oxidation to be used in air. Rhodium is more oxidation resistant than iridium although its melting temperature is somewhat lower (1985°C). Under certain conditions it can be used in oxidizing atmospheres, but our experience has shown it to be more susceptible than platinum to attack by iron oxide melts. Alloys of platinum with 3%, 10%, and 20% rhodium were used in crucibles, and although more resistant to deformation by the weight of the melt, the samples contained in crucibles with higher rhodium content did show more evidence of contamination. The degree of contamination as indicated by spectrographic analysis was of the order of 0.01 to 0.1% for both platinum and

rhodium with a preferential solution of rhodium over platinum of about five to one judging from the original alloy composition. Additional evidence for corrosion was found in leafy aggregates of metal crystals generally concentrated just below the melt surface on the crucible wall. In using the induction heating source the higher temperatures and greater convection led to greater contamination with suspension of the metal platelets in both melt and crystalline boules. The contamination problem was greatly reduced by the use of a pure platinum liner in contact with the melt. To avoid strain-induced recrystallization and the resulting premature failure of the platinum, a container crucible of rhodium or rhodium alloy was used.

Of the various oxides investigated as potentially useful crucible material, only yttrium oxide seemed promising. Yttrium oxide was considered not only a good refractory material (melting point 2400°C), but is also more attractive from the viewpoint of minimizing contamination during growth of YIG. Crucibles of yttrium oxide were prepared by slip casting and firing to 1900°C in a gas-oxygen kiln. The composition corresponding to the eutectic for the air isobar (13. 5 % Y_2O_3, 86. 5 % Fe_2O_3) was placed in the crucible which was then heated up to approximately 1500°C. The oxide melt gradually attacked the yttria crucible precipitating out the garn phase along the crucible wall. The attack was most extensive at the contact of the liquid surface and crucible wall. An initial reaction zone between yttria and yttrium iron garnet was composed primarily of yttrium orthoferrite ($YFeO_3$), but at the temperature of the firing only garnet is stable in direct contact with the liquid and no orthoferrite would grow in this region. The usefulness of this technique in crystal growing requires that the rate of solution of the crucible material by the oxide liquid is relatively slow. Ideally the rate of crystal growth should match the rate of solution of the yttria crucible. Since the use of this technique introduced additional experimental difficulties, it was decided to use the platinum alloy crucibles and to determine the proper conditions for growth before attempting the more complicated problem of matching growth and solution rates.

The method used to grow YIG in this investigation was to select a starting composition between 13. 5% and 22. 5 mole % Y_2O_3, the balance being Fe_2O_3, and liquify the oxide mixture by heating in a platinum crucible in air to above the liquidus temperature. The liquidus temperature differs for each starting composition and can be estimated from the liquidus curve for the air isobar (Fig. 1).

The crucible containing the charge was positioned in the furnace so that the melt surface was at a lower temperature than at any point below the surface, but hot enough to avoid freezing over. The gradient within the liquid could be varied with position, but was always kept hottest at the bottom of the crucible to avoid crystallization of garnet in this region. The increasing gradient from the surface downward also favored the formation of convection currents within the liquid, greatly enhancing the rate of material transport within the liquid.

Crystallization at the melt surface was brought about by immersing the tip of a platinum wire in the melt and lowering the temperature to the point where crystal growth took place on the wire. It was found that in air the surface tension of the oxide melt would support a meniscus about one-quarter inch in height before breaking contact with the melt. Surface tension and meniscus height decreased with higher oxygen pressure. After making contact between platinum wire and melt, the crystal was raised about one-eighth inch and rotation and pulling commenced.

Due to the large radiation losses at the melt surface, the vertical temperature gradient near the surface could be kept relatively high, but a desired radial gradient from the crucible wall decreasing to a small, relatively cool central area was far more difficult to achieve. In practice, a gradient from sidewall to center was one-tenth or less the vertical gradient and as a result, the YIG crystallized had a tendency to assume the flat shape of the temperature isotherms. Crystals of large diameter were difficult to manage and would often twist or break the wire, or make contact with the crucible wall.

Furthermore, continued growth in the vertical direction was inhibited by rising temperatures resulting from the blanketing effect of the crystal already grown. Lowering the temperature at this point would cause polycrystalline growth, whereas maintenance of the status quo would lead to reduced growth and eventual loss of contact. Thus it became impractical to try to grow single crystal YIG more than about one-eighth inch in thickness, although the diameter could be made to approach the surface area of the melt in the 40 ml crucible. The maximum rate of sound crystal growth was about 0.004 inch /hour.

To grow crystals of any reasonable length, it was evident that better control of the diameter of the YIG crystals would be required, which in effect meant a sharper radial temperature gradient as well as a sharp vertical gradient. Several schemes were tried to increase the radial gradient. One such measure was to construct a small disc shaped platinum wire wound heater with a hole in the center and to place this directly above the platinum crucible to heat the surface of the melt, except for the central region from which the crystal would be extracted. The second modification was to place a series of cylindrical platinum radiation shields concentrically in a region just above the melt surface so that the pulling rod and crystal would move into a relatively low temperature zone thereby increasing the crystal liquid interface gradient. A third variation was to place a spiral of platinum tubing within the innermost radiation shield and to blow air through the tubing so as to cool the central region just above the melt surface. The air flow was confined in the tubing and did not enter the reaction zone of the furnace.

Although all of these modifications seemed to be steps in the right direction, and a number of disc shaped crystals were grown, none were adequate to improve the gradient at the solid liquid interface to the point where the rate of sound crystal growth in the vertical direction was reasonably fast. Faster pulling rates were possible, but invariably led to a degeneration of the planar interface and inclusion of quenched liquid phase between dendritic spikes of YIG. Crystals produced by the final modifications of the gradient in the resistance furnace were grown at the rate of approximately 0.01 inch per hour. Considering the time necessary to monitor the crystal growth,

pulling rates of this order were considered too slow to be practical. For this reason, it was decided to abandon the use of the resistance heated furnace with its limited thermal gradients and to use an induction heating unit in which presumably much sharper temperature gradients could be attained by direct coupling to the crucible wall. With this arrangement, thermal insulation could be eliminated entirely and the temperature gradients increased through radiation losses.

A 20 kw, 450 kc induction unit was used for the rf crystal growth. The platinum crucibles previously used in the resistance heated pulling furnace had walls too thin (0. 010 in) for use with the induction unit, and several failed due to the formation of hot spots. To relieve this problem, platinum-rhodium alloy crucibles with a wall thickness of 0. 030 inch were tried, and they also failed after a very short period of operation. Next, a pure rhodium crucible whose wall thickness (0. 050 in) was calculated to be about three or four times the skin depth of the rf field was tried. Prior to using this crucible for crystal growth, the rate of attack by oxide liquid was tested by immersing a small strip of rhodium in oxide melt contained in a platinum crucible. After five hours at 1550°C, the rhodium strip had lost approximately 10% of its weight which is far beyond a tolerable rate of corrosion. Since pure platinum is more resistant to corrosion, a platinum liner was placed between the melt and the rhodium crucible. The liner was made to fit closely within the rhodium crucible to maintain good thermal contact and to support the relatively weak platinum. This particular arrangement has been the most successful of the various modifications attempted, although corrosion by the melt is still a limitation. The final crystal growing arrangement is shown schematically in Fig. 12. Radiation losses at the surface are controlled by the size of the opening in the refractory just above the crucible. The crucible is surrounded by a rhodium shield with a slit to decrease its coupling efficiency with the rf. Refractory brick surround the water cooled copper induction coil to minimize heat loss.

As expected, the use of induction heating did allow faster growth rates of YIG than those attainable in the resistance furnace unit with its smaller gradients. The growth rate of YIG using induction heating is approximately

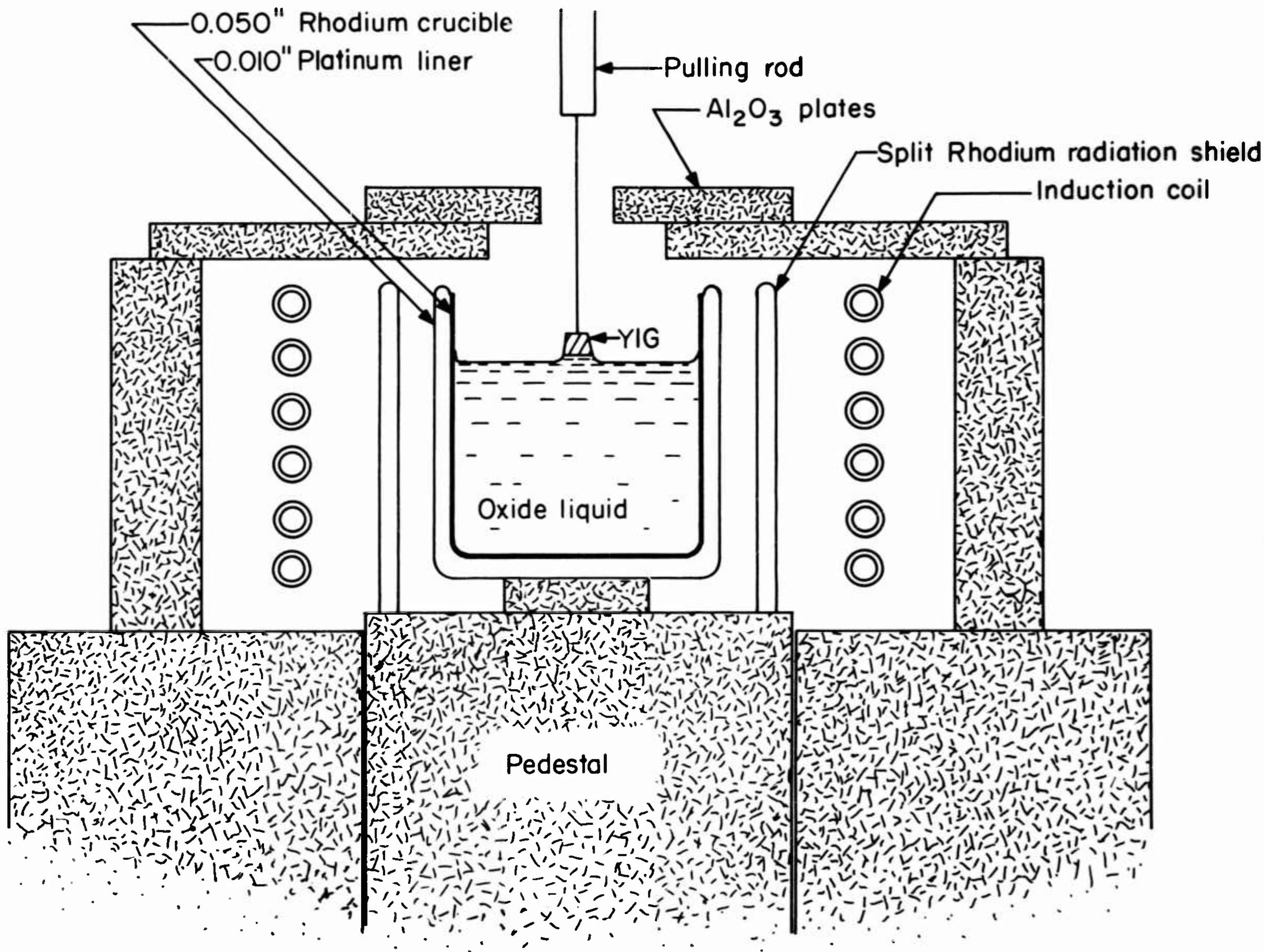

INDUCTION HEATED CRYSTAL PULLING UNIT
FIGURE 12

0.04 inch/hour at 1520°C with a crystal-liquid interface gradient of about 25°C. Higher growth rates lead to a breakdown of the planar interface and result in the inclusion of quench phase within the crystal. Experience has shown that temperature fluctuations greater than a few degrees cannot be tolerated during growth. A photograph of one such YIG crystal approximately one-half inch in diameter grown in this manner is shown in Fig. 14. However, the use of rf heating also resulted in more rapid attack of the platinum by oxide liquid through higher wall temperatures and increased thermal convection in the melt. With a fresh charge of oxide starting composition, crystals could be grown essentially free of metallic inclusions. As the growth interval lengthened, platinum was precipitated as leafy dendrites on the relatively cold surface of the growing boule. Corrosion of the platinum crucible also took place in the resistance furnace arrangement, but was less severe and did not result in contamination of the YIG crystallized.

Although faster pulling rates can be used with rf heating, the increased attack on the platinum crucible appears to counteract this advantage. Crystals have been grown free of metal inclusions in the resistance furnace, but in this case the maximum rate of growth of sound YIG free of quench phase is about 0.01 inch/hour, which is very slow with constant monitoring necessary. Thus, the combined effects of corrosion and slow reaction kinetics do not favor Czochralski growth in noble metal crucibles. The growth of YIG single crystals using one of the techniques which does not require a metal containing crucible appears to hold greater promise since higher temperatures and higher thermal gradients could be used without risk of contamination.

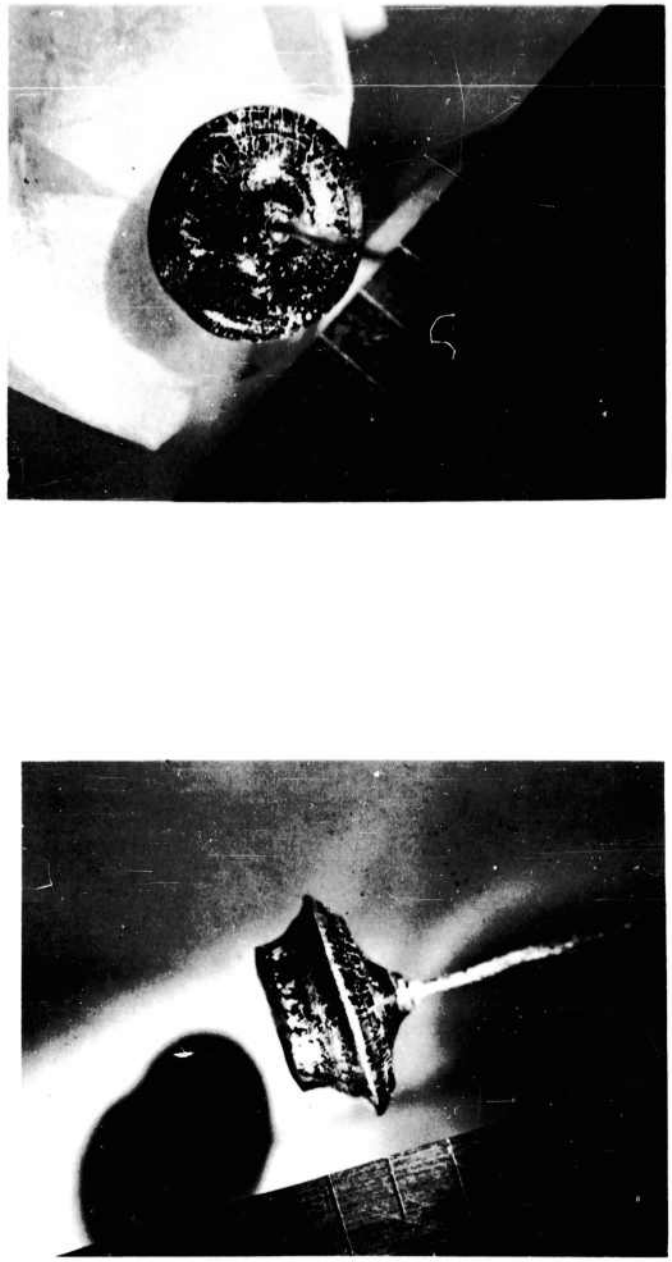

CZOCHRALSKI GROWN YIG SINGLE CRYSTAL

FIGURE 13

III. SPINEL SYSTEMS

A. Introduction

Phase equilibrium studies in spinel systems have been restricted to those where magnetite derived solid solutions appeared suitable for simple analysis of the valency exchange conductivity process. Solid solutions of the form $Fe^{+2}_{1-y}Me^{+2}_{y}Fe^{+3}_{2}O_4$ are the simplest substitution to consider, particularly when the divalent cation, Me^{+2}, locates only on one of the two types of sites available (tetrahedral or octahedral). Nickel and cobalt substitute exclusively in the octahedral sites where the conductivity is presumed to take place. Phase relations inthe systems Fe-Ni-O,[23] FeO-NiO-Fe_2O_3,[1] and Fe-Co-O[24] have been previously reported. Analysis of the results obtained with the nickel substitution have been previously described on one set of samples,[1] and additional data obtained on a set of samples prepared by a new technique will be discussed below.

Magnesium is a third type of divalent substitution that can be made in magnetite, and an additional feature is present in this system. The magnesium ion substitutes on either site, and the distribution between the octahedral and tetrahedral sites is temperature dependent. Consequently, at any fixed magnesium concentration, the number of ferrous and ferric ions participating in the octahedral conduction process can be varied by suitable heat treatment. This system should allow for checking the validity of the assumption that the electron hopping occurs exclusively via octahedral sites. Phase relations in the system FeO-MgO-Fe_2O_3[25] have been previously described, and the temperature dependence of the cation distribution in non-stoichiometric magnesium ferrite is described in a following section.

One final type of substitution that was considered is represented by $Fe^{+2}Fe^{+3}_{2-y}Al^{+3}_{y}O_4$, where the carriers are maintained constant, but the octahedral sites containing trivalent iron for conduction are dependent upon the value of y. In this system, as with the previous one, the cation distribution

is temperature dependent and, at constant composition, the ferric ions participating in octahedral conduction can be varied by proper heat treatment. Phase relations obtained in this system are presented below.

B. Phase Equilibria in the System FeO-Fe_2O_3-Al_2O_3

1. Introduction

Divalent substitution of nickel in Fe_3O_4 extends the binary magnetite field to a terminal composition corresponding to $NiFe_2O_4$. Cobalt likewise will substitute for divalent iron through $CoFe_2O_4$ to Co_3O_4. In both systems, the spinel field narrows very rapidly when it is extended into the ternary diagram. In the vicinity of $NiFe_2O_4$ and $CoFe_2O_4$, the field has little or no width.[23, 24]

In contrast to the latter two systems, the spinel field in the ternary system FeO-Fe_2O_3-Al_2O_3 has considerable width starting at Fe_3O_{4+x} through $FeAl_2O_{4+x}$.[13, 14] Richards and White[14], in fact, show that ternary spinel solid solutions in air up to 1500°C have oxygen contents greater than the maximum value in magnetite at equivalent temperatures. This indicates that much lower oxygen pressures are required to prepare solid solutions along the stoichiometric join, Fe_3O_4-$FeAl_2O_4$, than was required in either of the former two systems where pressures in the range of 10^{-3} atmospheres or higher were required. Consequently, gas mixtures of CO and CO_2 were required to generate oxygen pressures below 10^{-3} atmospheres. The phase equilibrium studies in this system were carried out at 1300°, 1400° and 1500°C in CO_2 and at 1500°C over a range of oxygen pressures in order to define the conditions necessary to prepare stoichiometric solid solutions.

2. Experimental Procedure[1]

The starting mixtures of Al_2O_3 and Fe_2O_3 were made by co-precipitating the desired Fe:Al ratio as hydroxides. Chemical analysis was performed after an initial 12 hour calcining at 1000°C in oxygen. The material was

screened, pressed, and reacted a second time at 1300°C in air and slowly cooled to room temperature. Small samples were packed in platinum-rhodium vials, equilibrated at various temperatures and oxygen pressures for times ranging up to 24 hours and water quenched. Phase identification and lattice parameter measurements were made using iron filtered cobalt radiation. Porous pressed samples were suspended by means of a thin alumina rod at the thermal center of the thermobalance furnace for determining ternary compositions. The other end of the rod was attached by platinum wire to a pan of the automatic recording balance.

Mixtures of CO_2 and CO used to produce the low oxygen partial pressures were purified and mixed in an apparatus similar to the one described by Kingery.[26] A schematic diagram of the apparatus is shown in Fig. 14. The impurities in the carbon dioxide were removed by passing the gas over silica gel to remove hydrogen sulfide and sulfur dioxide, hot copper oxide to remove oxygen, hydrogen and carbon monoxide; and through a cold trap (dry ice + alcohol) to remove water vapor. The impurities in carbon monoxide were removed by passing the gas over re-ignited asbestos (500°C) to remove iron carbonyl, silica gel to remove hydrogen sulfide and sulfur dioxide, heated copper to remove hydrogen and oxygen; and through a cold trap (dry ice + acetone) to remove water vapor and carbon dioxide. Orsat gas analysis of the CO_2 - CO mixtures was in good agreement with the values obtained from the flowmeter readings.

3. Results and Discussion

The ternary diagram for the CO_2 isobar at 1300°C, 1400°C, and 1500°C constructed from the data in Tables IV and V is illustrated in Fig. 15. It is evident that oxygen pressures below that produced by CO_2 decomposition even at the highest temperature employed (1500°C, 1.8×10^{-3} atmospheres of oxygen) are required to produce stoichiometric spinels on the Fe_3O_4-$FeAl_2O_4$ join. Equilibration times in this system at the lower temperatures were extremely long so that most of the additional effort was concentrated on obtaining

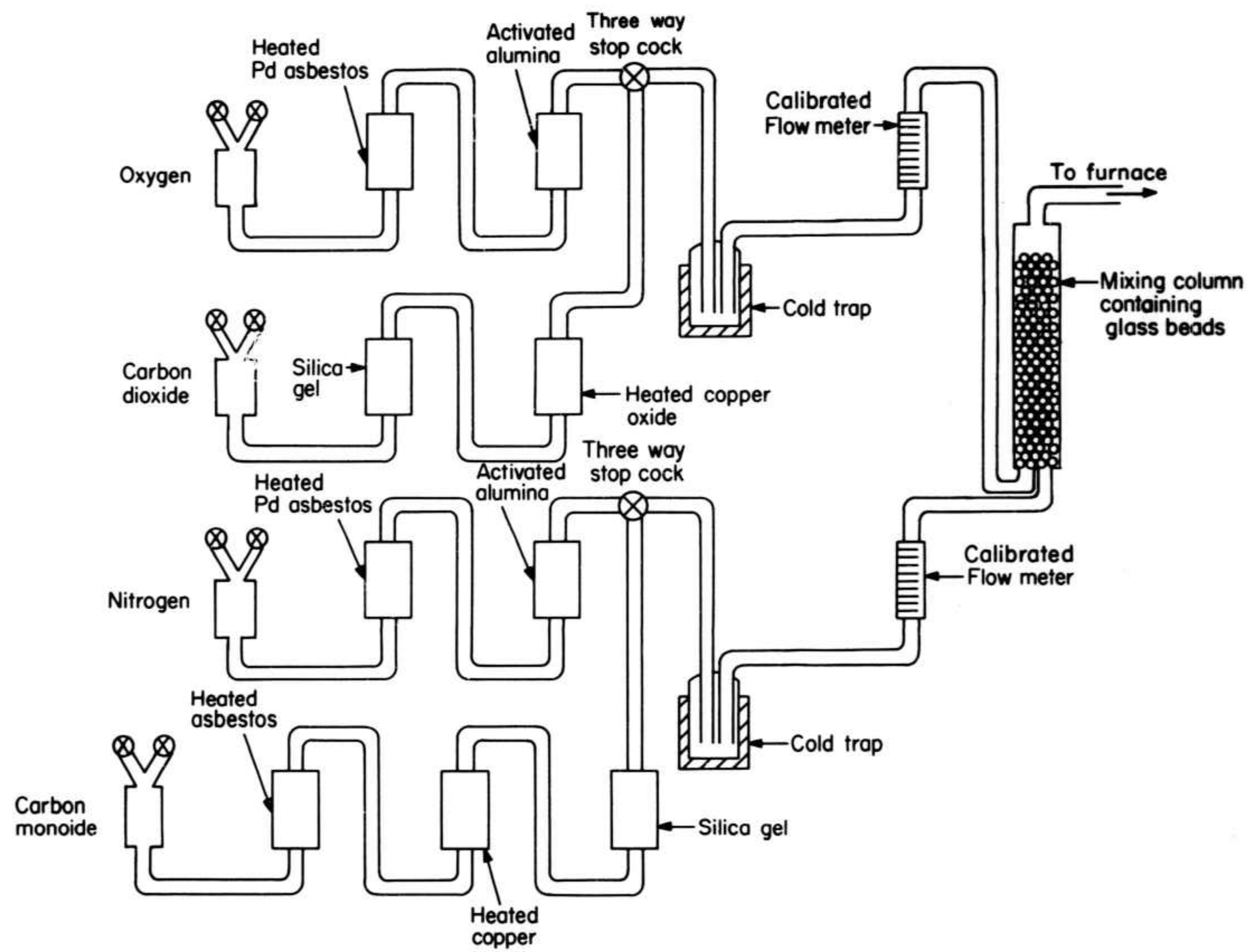

SCHEMATIC DIAGRAM OF GAS PURIFICATION AND MIXING APPARATUS
FIGURE 14

TABLE IV

Phase Identification of Quenched Samples in CO_2

for the System $FeO-Fe_2O_3-Al_2O_3$

Initial Composition Mole % Al_2O_3	Temperature 1300°C	1400°C	1500°C
7.0	spinel a = 8.3740±.0005	------	spinel a = 8.3753±.0005
16.4	spinel a = 8.3378±.0005	------	spinel a = 8.3404±.0005
32.1	spinel a = 8.3001±.0005	------	spinel a = 8.2879±.0005
41.3	spinel + corundum	spinel	------
47.5	------	------	spinel a = 8.2306±.0005
55.5	spinel + corundum	spinel a = 8.2578±.0005 + corundum	spinel a = 8.2042±.0005
62.9	------	------	spinel a = 8.2016±.0005 + corundum
67.7	spinel a = 8.315±.001 + corundum	spinel a = 8.258±.002 + corundum	------

TABLE IV (Continued)

Initial Composition Mole % Al_2O_3	Temperature 1300°C	1400°C	1500°C
68.3	- - - - - -	- - - - - -	spinel a = 8.201±.001 + corundum
69.1	spinel a = 8.315±.002 + corundum	spinel + corundum	- - - - - -

TABLE V

Equilibrium Compositions in CO_2 for the System FeO-Fe_2O_3-Al_2O_3

Initial Composition Mole %	1300°C Mole %			1400°C Mole %			1500°C Mole %		
Al_2O_3	FeO	Fe_2O_3	Al_2O_3	FeO	Fe_2O_3	Al_2O_3	FeO	Fe_2O_3	Al_2O_3
7.0	---	----	----	---	----	----	49	46	5
11.3	46.0	45.0	9.0	48.0	43.5	8.5	---	----	----
22.2	45.5	37.5	17.0	---	----	----	---	----	----
32.1	40.5	34.0	25.5	46	29	25	48.5	27.0	24.5
41.3	---	----	----	---	----	----	47.5	21	31.5
47.5	32.0	28.5	39.5	38.0	23.5	38.5	45.0	18.0	37.0
55.5	---	----	----	---	----	----	43.0	13.5	43.5
62.9	---	----	----	---	----	----	38.5	11.0	50.5
67.7	18.5	20	61.5	23.0	17.0	60	32.0	11.0	57.0
85.8	6	11	83.0	9.0	9.0	82.0	10.5	8.0	81.5

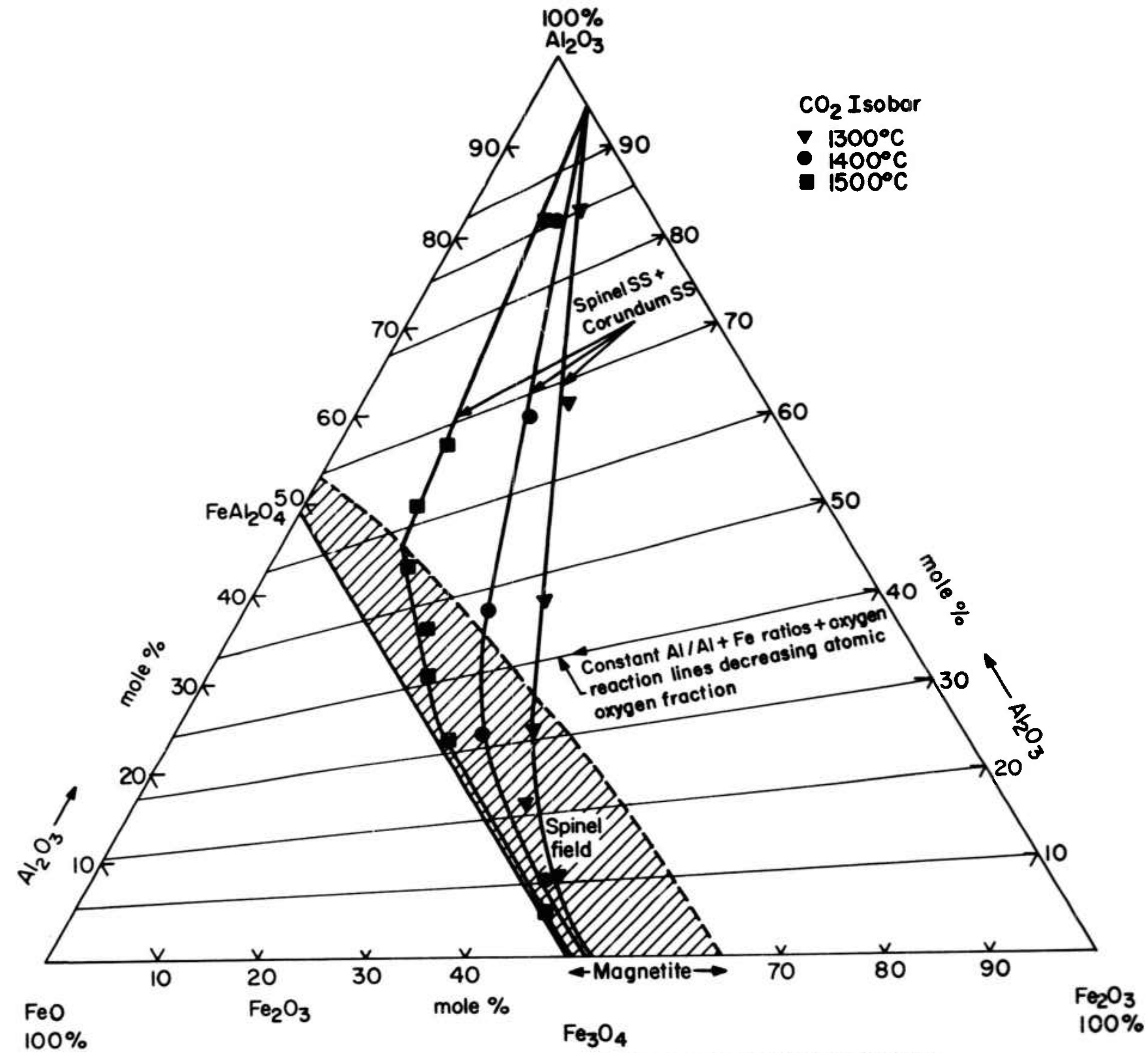

THE CO_2 ISOBAR AT 1300°C, 1400°C AND 1500°C IN THE TERNARY DIAGRAM $FeO - Fe_2O_3 - Al_2O_3$

FIGURE 15

TABLE VI

Phase Identification of Quenched Samples at 1500°C

for the System $FeO-Fe_2O_3-Al_2O_3$

Initial Composition Mole % Al_2O_3	Oxygen Partial Pressure 4×10^{-7} atmosphere	Oxygen Partial Pressure 7×10^{-10} atmosphere
32.1	spinel a = 8.2232±.0008 + quench phase	- - - -
52.0	spinel a = 8.2232±.0005	spinel a = 8.1705±.0005 + wüstite type quench phase
55.5	spinel	spinel a = 8.1705±.0005 + wüstite type quench phase
62.9	spinel a = 8.1798±.0001	spinel a = 8.1683±.0005
67.7	spinel a = 8.1426±.0003	spinel a = 8.1471±.0005
68.3	spinel a = 8.1425±.0005	spinel a = 8.1397±.0005
69.1	spinel + corundum	spinel a = 8.1323±.0006 + corundum
71.9	- - - -	spinel a = 8.1319±.0005 + corundum
80.4	- - - -	spinel a = 8.1312±.0005 + corundum
85.8	spinel + corundum	

TABLE VII

Equilibrium Compositions at 1500°C for the System $FeO-Fe_2O_3-Al_2O_3$

Initial Composition	Partial Oxygen Pressure 4×10^{-7} atmosphere			7×10^{-10} atmosphere		
Mole % Al_2O_3	Mole % FeO	Mole % Fe_2O_3	Mole % Al_2O_3	Mole % FeO	Mole % Fe_2O_3	Mole % Al_2O_3
39.1	59.0	13.5	27.5	---	----	----
52.0	50.0	10.5	39.5	---	----	----
55.5	50.0	8.0	42.0	60.5	0.5	39.0
62.9	49.0	3.5	47.5	53.5	0.5	46.0
67.7	46.0	2.0	52.0	---	----	----
68.3	---	----	----	47.0	0.5	52.5
69.1	44.5	2.0	53.5	---	----	----
71.9	39.5	2.5	58.0	42.5	0.5	57.0
80.4	29.5	2.0	68.5	32.0	0.5	67.5
85.8	22.0	1.5	76.5	---	----	----
88.6				18.0	1.5	80.5

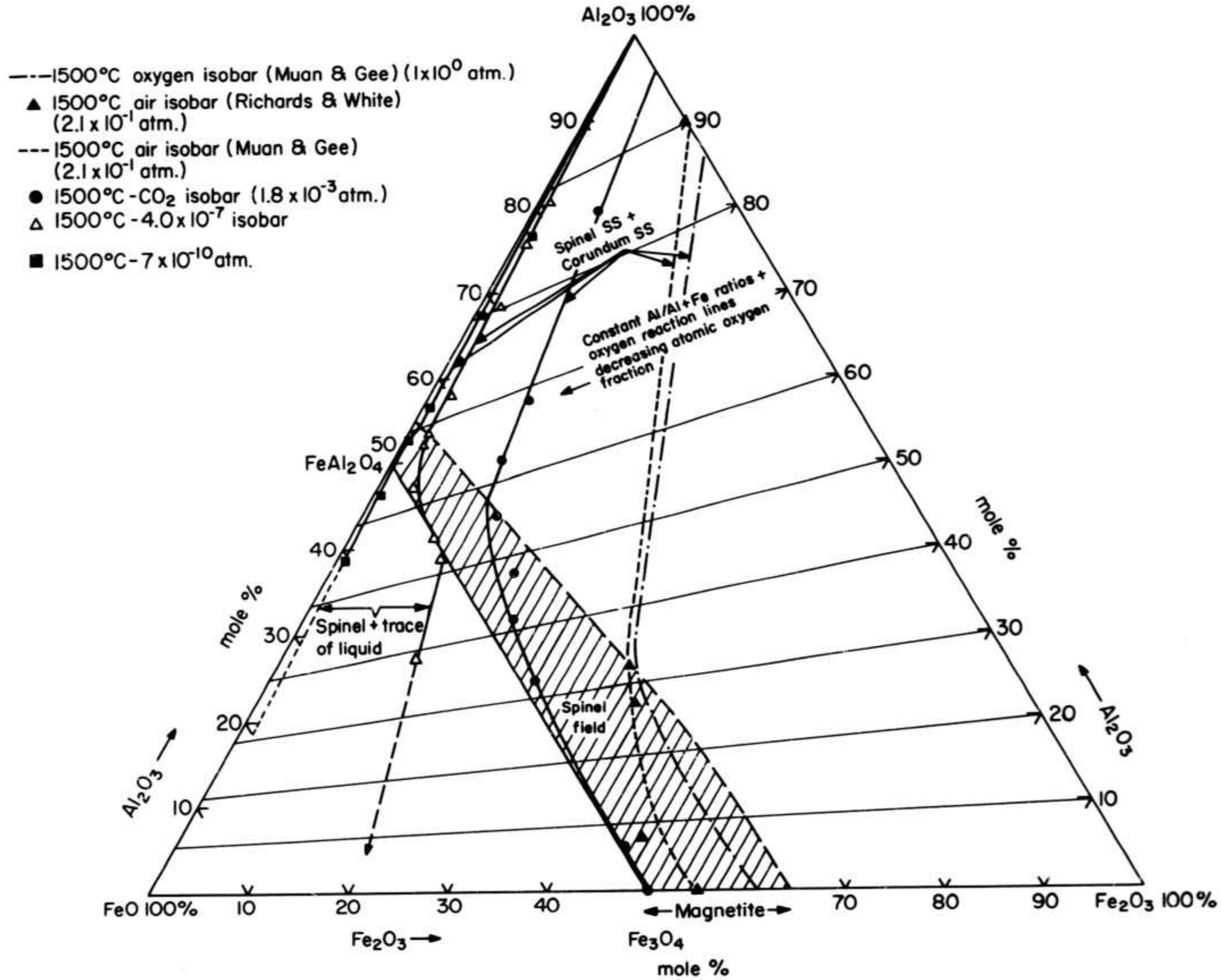

THE 1500 °C ISOTHERMAL SECTION IN THE SYSTEM $FeO - Fe_2O_3 - Al_2O_3$

FIGURE 16

low pressure data at 1500°C. In a later section, a technique for obtaining dense stoichiometric samples from limited phase equilibria data will be discussed from which it will be clear that the 1500°C data is sufficient for preparing Fe_3O_4-$FeAl_2O_4$ solid solutions.

The 1500°C isothermal section constructed from data in Tables VI and VII is illustrated in Fig. 16. Spinels along the Fe_3O_4-$FeAl_2O_4$ join can be prepared in oxygen pressures from 1.8×10^{-3} atmosphere to slightly less than 7×10^{-10} atmosphere. The spinel field extends from the binary magnetite field into the ternary system with considerable width, in contrast to several systems reported earlier.[23-25] At 1500°C, the maximum width of the spinel field of the binary system FeO-Al_2O_3 is 53.0 mole percent Al_2O_3 and 47.0 mole percent FeO (compared to 50-50 for $FeAl_2O_4$). This compared to Hoffman and Fisher's[27] data at 1750°C: 56.5 mole percent Al_2O_3 and 43.5 mole percent FeO. The two binary systems FeO-Fe_2O_3 and FeO-Al_2O_3 behave quite similarly. With increasing temperature, the spinel field in each case widens in the direction of increasing oxygen content.

C. Cation Distribution in Non-Stoichiometric Magnesium Ferrite

1. Introduction

The cation distribution in magnesium substituted magnetite solid solutions must be determined in order to define the ratio of Fe^{+3} to Fe^{+2} on octahedral sites where electron hopping presumably occurs. In particular, the temperature dependence of the distribution parameter η, defined as the fraction of magnesium ions on tetrahedral sites, is desired. Magnetic moment and X-ray intensity measurements have been made to determine the distribution parameter on the terminal composition in this series. Measurements on other compositions are currently in progress.

2. Previous Studies on Magnesium Ferrite

The overall structural features of magnesium ferrite are well known.[28-31] It has the spinel crystal structure with a partially inverted cation distribution whose degree of inversion is temperature dependent. Results in the literature, however, are not in close agreement on the exact form of this temperature dependence. Bertaut[29] used X-ray diffraction methods to measure the cation distribution in samples of magnesium ferrite quenched from various temperatures. He observed a decrease in the degree of inversion from nearly 100% at room temperature to about 78% at 1200°C. Pauthenet and Bochirol[32] made more detailed determinations from saturation magnetization measurements and found that their results followed a distribution law of the form

$$\eta (1 + \eta)/(1 - \eta)^2 = e^{-\theta/T}$$

where η is the fraction of Mg ions occupying tetrahedral sites (the degree of inversion in $MgFe_2O_4$ would be $100 (1 - \eta)$ %) and θ is a constant equal to 1200°K. More recent magnetization measurements by Kriessman and Harrison[33] and by Epstein and Frackiewicz,[34] on the other hand, indicated that θ has the form $\theta = \theta_o - \theta_1 \eta$ where θ_o and θ_1 are constants. The results of the latter investigators are in general agreement but the respective values of η as a function of temperature, and of θ_o and θ_1, differ somewhat.

Kriessman and Harrison[33] have cited two factors which may be partially responsible for the discrepancies which exist in the saturation magnetizations reported by various authors for similar quench temperatures. These are the difficulties in obtaining true equilibrium conditions for the highly refractory magnesium ferrite, and in quenching sufficiently rapidly to preserve the arrangement of atoms which prevailed at the firing temperature. Additional complications are inferred by the phase equilibria studies in the ferrite region of the system FeO-MgO-Fe_2O_3.[25] These studies have shown, for example, that Mg^{++} replaces Fe^{++} in Fe_3O_4 beyond the "stoichiometric $MgFe_2O_4$" to $(MgO)_xMgFe_2O_4$ (where $x = 0.092 \pm .004$) and that the extent to

which distribution changes occur as a function of temperature depends markedly on the magnesium concentration in the spinel. Consequently, small differences in the relative amounts of MgO and Fe_2O_3 used in the sample preparation would be reflected in the measured cation distributions. Furthermore, the spinel field was not found to include a single-phase composition corresponding to $MgFe_2O_4$. The significance of the determination of a structural property such as the cation distribution is therefore intimately associated with the accuracy to which the composition is known, as well as how closely the sample is representative of equilibrium conditions.

The following sections summarize data obtained on the temperature dependence of certain crystallographic properties of non-stoichiometric magnesium ferrite in the range from room temperature to 1100°C. The quantities investigated were the lattice parameter (a), the oxygen position parameter (u), the cation distribution (η), and the density (ρ). The variation of a, u, and η with quench temperature was measured by X-rays, and the η's were independently determined from saturation magnetization measurements. The densities were obtained from pycnometric measurements. These quantities provide sufficient information for a description of the spinel structure on a statistical basis. The location of ionic sites within the lattice are fixed by a and u while η describes the way in which the cations are distributed. The nature of lattice defects, whether they are interstitial Mg (or Fe) ions or oxygen vacancies, should be implied from the density.

3. Defect Structures of Non-Stoichiometric Magnesium Ferrite

Non-stoichiometric magnesium ferrite, $(MgO)_x MgFe_2O_4$ must have one of two types of defects present: (1) the oxygen lattice is complete while the excess metal ions are distributed among the 16 unoccupied octahedral and 56 unoccupied tetrahedral sites, or (2) the metal lattice is complete while vacancies occur in oxygen lattice. For case (1), we can write

$$Mg_{1.0 + 2n} Mg\Delta_n Fe_{2 - 2n} O_4$$

where $Mg\Delta_n$ represents an excess of magnesium by an amount n. The n $Mg\,\Delta$ ions are required for electroneutrality and n is related to x by

$$n = \frac{x}{x+4} \quad . \tag{1}$$

The formulas corresponding to case (2) can be expressed as $Mg_{1.0+2\delta}Fe_{2-2\delta}O_{4-\delta}[o.v.]_\delta$ where [o. v.] are oxygen vacancies of an amount δ, which is related to x by

$$\delta = \frac{x}{x+3} \quad . \tag{2}$$

The net magnetic moment in Bohr magnetons per molecule is given by the difference between the sum of the moments on the octahedral and tetrahedral sites,

$$m = m_{oct} - m_{tet} \quad . \tag{3}$$

For the anion vacancy case, the distribution of magnesium ions over the tetrahedral and octahedral sites is simply $(Mg_yFe_{1-y})[Mg_{1+2\delta-y}Fe_{1+y-2\delta}]$ and the magnetic moment is given by

$$m_1 = 5\,[(1+y-2\delta)-(1-y)] \quad . \tag{4}$$

Therefore, from saturation moments, the value of y can be determined, and hence the fraction of magnesium ions on tetrahedral sites, or η, can be evaluated.

For the interstitial case, the distribution may be written $(Mg_yFe_{1-y})[Mg_{1+2n-y}Fe_{1+y-2n}]\,Mg\Delta_n$ where the $Mg\Delta$ are assumed to occupy positions which are normally vacant in a spinel lattice. The net magnetic moment is then given by $m_2 = 5\,[(1+y-2n)-(1-y)]$. In reality the type and positions of the interstitial cations (Mg or Fe) remains undetermined because they are too few to have a significant effect on the X-ray intensity

measurements. Nevertheless it will be shown that geometric considerations favor the location of these ions at octahedral positions. Our calculations of η from the magnetic measurements assumes such a positioning and also that the direction of the magnetic moment at these sites is the same as in the normally occupied octahedral sites. However, in the event that the interstitial cations consist of Fe ions in tetrahedral sites, the calculations should be adjusted by a 0.02 increase in the magnetically determined η values.

It will be noted that δ and n are similar in value, 0.03 and 0.02 respectively, and the distribution parameter calculated from magnetic moment data using either the anion vacancy or interstitial cation model is almost identical. The results of the X-ray analysis are also the same for either case.

4. X-Ray and Magnetic Methods and Results

Samples were prepared by igniting mixed oxalate precipitates of magnesium and iron.[25] Chemical analysis was used to determine the metal ratio in the powders.

Saturation magnetization measurements were made on a vibrating sample magnetometer similar to the one described by Foner.[35] Dense sintered spheres of magnesium ferrite 1 - 2 mm in diameter, quenched from various temperatures, were measured as a function of temperature down to -195°C. Figure 17 is a plot of the data, and the magnetic moment was determined by extrapolation to absolute zero. The saturation moment values and distribution parameters calculated from

$$\eta = \frac{y}{1 + 2\delta} \tag{6}$$

$$\eta = \frac{y}{1 + 2n} \tag{7}$$

are listed in Table VIII.

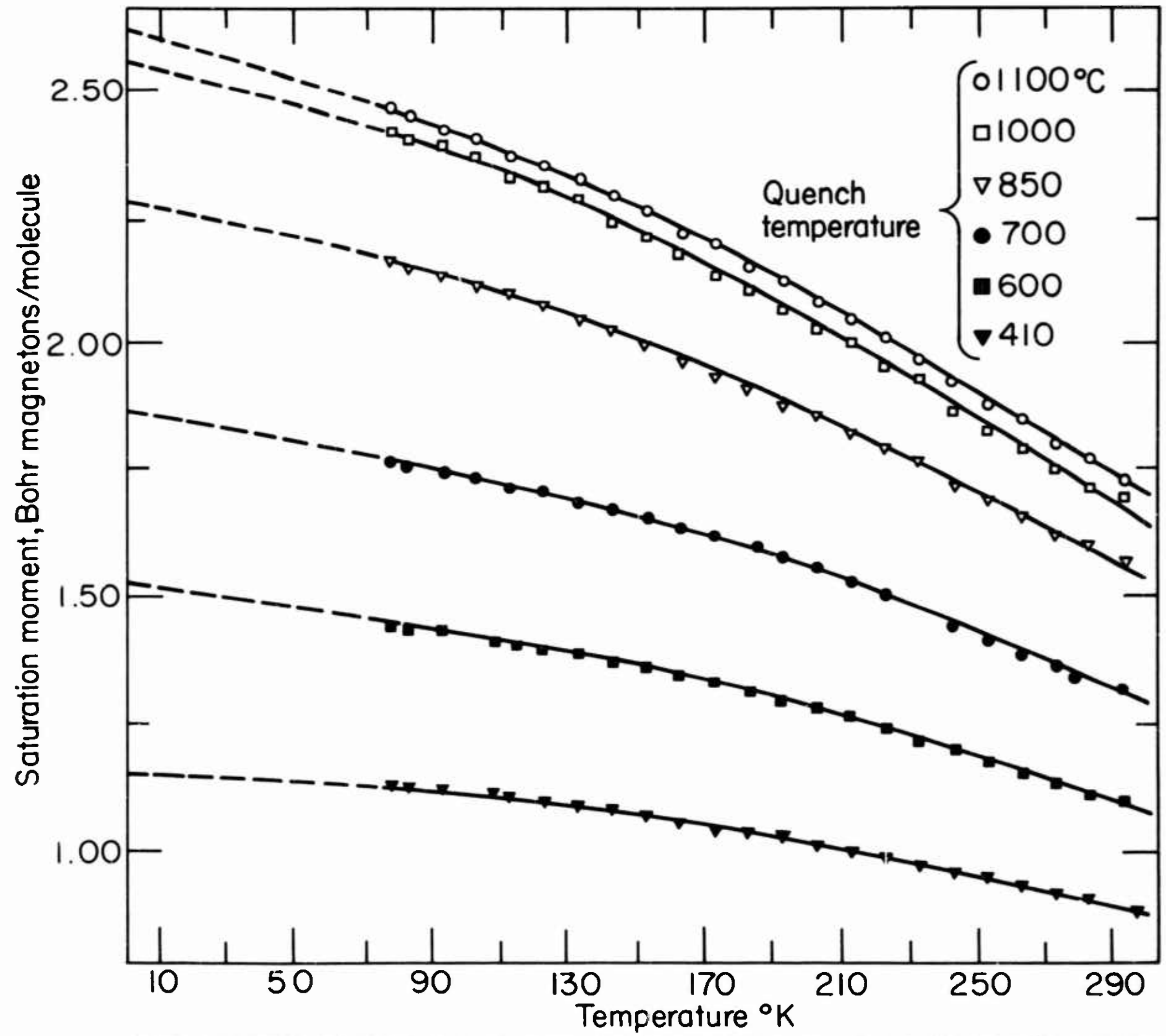

SATURATION MOMENT PER MOLECULE OF NON-STOICHIOMETRIC MAGNESIUM FERRITE AS A FUNCTION OF TEMPERATURE FOR DIFFERENT QUENCH TEMPERATURES

FIGURE 17

TABLE VIII

Saturation Moments and Distribution Parameters for Various Quench Temperatures for Non-Stoichiometric Magnesium Ferrite

Quench Temperature (°C)	Saturation Moment Bohr Magnetons/molecule	Distribution Parameter η Interstitials	Oxygen Vacancies
410	1. 15	0. 13	0. 13
600	1. 53	0. 17	0. 17
700	1. 86	0. 20	0. 20
850	2. 27	0. 24	0. 24
1000	2. 53	0. 26	0. 26
1100	2. 59	0. 27	0. 27

The X-ray measurements were made on a Norelco diffractometer using Fe-filtered $CoK\alpha$ radiation and Geiger counter detection. Powders quenched from each temperature were ground and packed as flat samples following the usual precautions to ensure random orientation of the crystallites. Diffraction scans were run in the 2θ range from 20° - 95° at 1° in 2θ per minute to verify that the powder was single-phased magnesium ferrite. The regions where the strongest MgO reflections would occur were scanned at 1/8° per minute. These reflections, the (200) and (220), would appear on the low angle side of the (400) and (440) spinel peaks but could be resolved at these scanning speeds. Lattice parameters of magnesium ferrite were determined from the 2θ positions of the (751) and (840) reflections. These measurements were calibrated with a silicon standard sample and were reproducible to within ±0.0005 A.

Diffraction line profiles were obtained automatically by the fixed-point, fixed-count step scanning technique with a Norelco counting rate computer. All (hkℓ) reflections up to and including the (531) were scanned at either 0.01° or 0.02° in 2θ per step and with at least 12,800 counts per point. The reproducibility of the intensity measurements, with regard to both the production and detection of X-rays and the sample packing, was checked by rescanning the (111) at intervals throughout the course of measurements on each sample. (The maximum deviation from the average (111) integrated intensity was found to be $8\frac{1}{2}\%$ with a more representative value being about 4%. These variations are consistent with the probable errors listed in the results). Each point on the line profiles was corrected for nonlinearity in the Geiger counter response[36] and the relative integrated intensities were obtained by evaluating the peak areas above background.

When measured by the diffractometer method, the integrated intensity of an (hkℓ) reflection from a flat powder sample is related to the crystallographic parameters through the formula

$$I = Am_{hk\ell} \frac{(1 + \cos^2 2\theta)}{\sin^2 \theta \cos \theta} F^2_{hk\ell} (u, \eta) \exp [-2B (\sin \theta/\lambda)^2] . \quad (8)$$

For the magnesium ferrite samples, which had the same chemical composition but different unit cell volumes (v), the proportionality constant may be written

$$A = K/v \tag{9}$$

where K is a constant for given diffractometer operating conditions. The factor $m_{hk\ell}$ in Eq. (8) is the multiplicity for $(hk\ell)$ planes and θ is the Bragg angle, $F_{hk\ell}$ is the structure factor, B is an average Debye-Waller temperature factor, and λ is the X-ray wavelength.

The values of A, η, u, and B which gave a best fit between the calculated (I_c) and observed (I_o) relative integrated intensities of the (111), (220), (311), (400), (422), (440), (511) and (333) reflections were determined by a least squares refinement for samples quenched at 1100°, 700°, and 410°C. (The sum of the (511) and (333) reflections was measured since they are superimposed in a powder pattern). The computations were carried out on an IBM 704 computer by means of a program devised by Dr. O. J. Guentert of this laboratory, which utilizes an iteration procedure to derive the parameters that minimize the quantity

$$\Sigma D^2 = \sum_{hk\ell} \frac{(I_c - I_o)^2}{I_o^2} \quad . \tag{10}$$

The scattering factors used in the calculations were those of Berghius et al.[37] for Mg^{+2}, of Watson and Freeman[38] for Fe^{+3}, and of Freeman[39] for O^{-2}. Dispersion corrections, considering only contributions from the K electrons, were made according to the methods of Parratt and Hempstead.[40] The imaginary components were found to be negligible and the corrections, in electron units, applied to the scattering factors of Mg^{+2}, Fe^{+3} and O^{-2} were 0. 16, -3. 9, and 0. 4 respectively. The scattering from lattice defects. which are not numerous enough to make a significant contribution to the structure factor, was neglected.

The weighting factor of $1/I_0^2$ used in this program would over-estimate the reliability of the weak (222), (331) and (531) reflections and they were consequently omitted. Standard deviations were calculated from

$$\sigma(\zeta_i) = \left(\frac{\Sigma \quad D^2}{(m-s) \sum\limits_{hk\ell} (\partial D/\partial \zeta_i)^2} \right)^{\frac{1}{2}} \qquad (11)$$

where m is the number of hkℓ reflections and s is the number of parameters determined.

The diffraction patterns for all samples were consistent with single phase spinels having the lattice parameters listed in Table IX. No superstructure lines, signifying long-range ordering within the tetrahedral and (or) octahedral sites, were observed.

The results of the least squares determination of A, B, u, and η are summarized in Table X. As might be expected, the A and B parameters were constant within the standard deviations (the variation in A to be expected from lattice parameter differences is only about $\frac{1}{2}$%). The Debye temperature, determined from B, is 490°±50°K in agreement with the result of Bacon and Roberts.[30] The u parameter was also independent of quench temperature and is in accord with the neutron diffraction values of Bacon and Roberts[30] and of Corliss, Hastings, and Brockman[31] who found u = 0.382±0.002 and 0.381±0.001, respectively. The standard deviations in u were felt to be unrealistic and they have been arbitrarily tripled in Table X. Table XI gives a comparison of the observed integrated intensities with those calculated using the refined parameters.

The temperature dependence of the distribution parameter, η, is plotted in Fig. 18 where the agreement between the two sets of data is reasonable. From the theoretical treatment of Callen, Harrison, and Kriessman[41] and using the assumptions of Kriessman and Harrison,[33] the cation distribution for a stoichiometric spinel of the composition $Mg_yFe_{3-y}O_4$ should have a temperature dependence of the form

TABLE IX

Lattice Parameters of Non-Stoichiometric Magnesium Ferrite for Various Quench Temperatures

T (°C)	a (A)
20	8.3851±.0005
410	8.3848
700	8.3896
800	8.3925
900	8.3954
1000	8.3969
1100	8.3983

TABLE X

Results of Least Squares Determinations

T (°C)	$A \times 10^5$	B (A^2)	u	η
410	1.31±0.02	0.55±0.1	0.381±0.001	0.12±0.01
700	1.31±0.02	0.51±0.1	0.381±0.001	0.22±0.01
1100	1.31±0.02	0.62±0.1	0.381±0.001	0.28±0.01

TABLE XI

Calculated and Observed Integrated Intensities

hkℓ	I_c (T = 410°C)	I_o (T = 410°C)	I_c (T = 700°C)	I_o (T = 700°C)	I_c (T = 1100°C)	I_o (T = 1100°C)
111	6. 7	6. 8	8. 5	8. 6	12. 2	12. 1
220	46. 8	47. 5	42. 9	43. 8	40. 0	41. 6
311	132. 6	138. 8	134. 2	136. 0	131. 2	130. 1
222	0. 6	0. 3	0. 7	0. 4	1. 0	0. 8
400	34. 9	34. 5	39. 1	38. 7	40. 5	40. 8
331	0. 0	0. 0	0. 2	0. 0	0. 2	0. 0
422	14. 2	13. 7	13. 3	12. 5	12. 2	11. 5
511-333	41. 8	42. 7	40. 9	42. 6	40. 5	41. 8
440	63. 3	65. 6	65. 1	66. 3	63. 4	64. 7
531	0. 8	0. 2	1. 0	0. 2	1. 3	0. 6

	T = 410°C	T = 700°C	T = 1100°C
ΣD^2	0. 0046	0. 0069	0. 0069

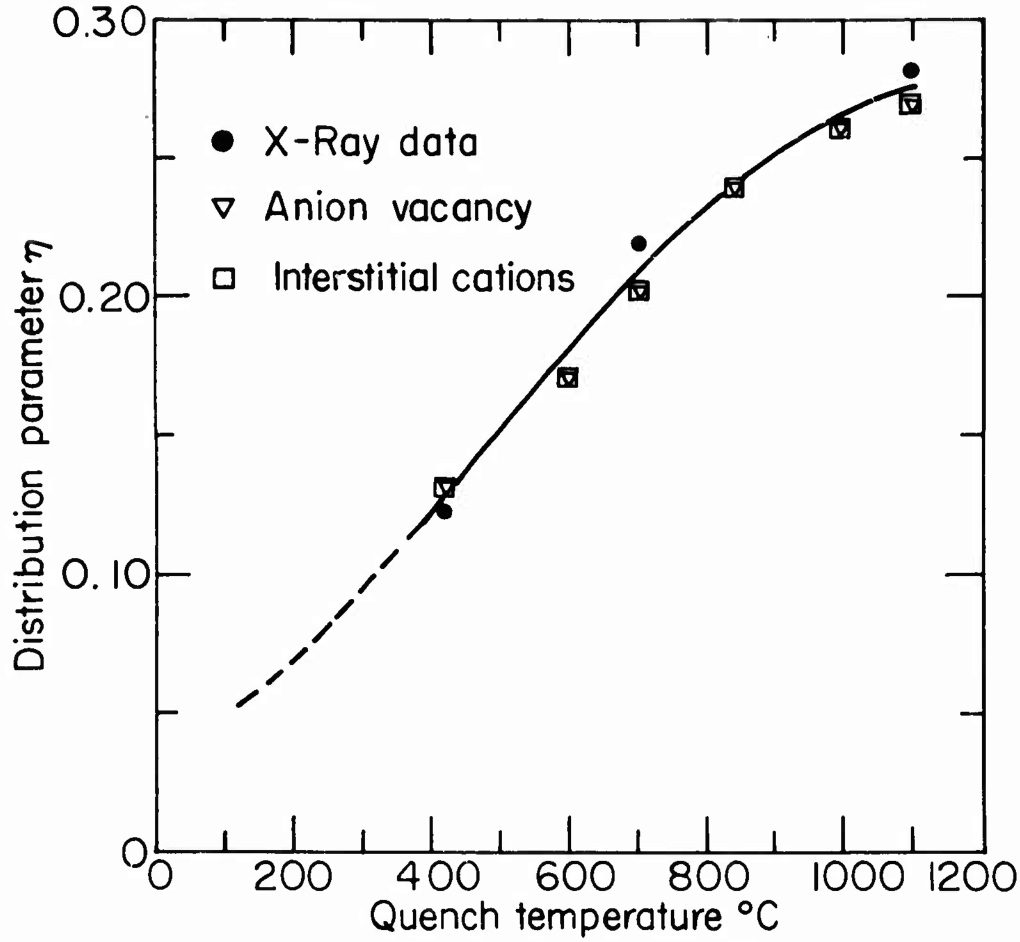

DISTRIBUTION PARAMETER η FOR NON-STOICHOMETRIC MAGNESIUM FERRITE AS A FUNCTION OF QUENCH TEMPERATURE. FILLED CIRCLES DETERMINED BY X-RAYS, OPEN SYMBOLS FROM MAGNETIC MOMENT DETERMINATIONS

FIGURE 18

$$\frac{\eta\,(2 - y + \eta y)}{(1 - \eta)(1 - \eta y)} = \exp\left[\frac{-1}{yRT}\,\frac{\partial u_1}{\partial \eta}\right] \qquad (12)$$

where u_1 is the non-thermal contribution to the energy, R is the gas constant per mole and T is the temperature in degrees K. The temperature dependence of η measured by Kriessman and Harrison and by Epstein and Frackiewicz[34] indicated that the quantity $1/R\ (\partial u_1/\partial \eta)$ can be expressed by

$$1/R\left(\frac{\partial u_1}{\partial \eta}\right) = \theta_o - \theta_1 \eta \text{, where } \theta_o \text{ and } \theta_1 \text{ are constants} \qquad (13)$$

The present results for magnesium ferrite confirm this relationship although they lead to different values of θ_o and θ_1 as shown in Table XII.

Pycnometric density measurements on several samples quenched from 1100°C did not give conclusive evidence of either anion vacancies or cation interstitials for non-stoichiometric magnesium ferrite. The theoretical density values for this quench temperature are 4.466 gms/cc for cation interstitials and 4.432 gms/cc for oxygen vacancies. Normally, a one percent difference should be distinguished by pycnometer density measurements. However, magnetic powders tend to agglomerate which prevents complete wetting. This results in consistently low density values. If a density measurement fell between the two figures quoted above, then it could be stated that the agreement was with the higher value, corresponding to cation interstitials. On the other hand, if the measured value was lower than both figures, it would be difficult to state unequivocally that the agreement was with the lower theoretical value. Even if the true situation corresponded to cation interstitials, measured values could be low by an amount that would place them below the calculated anion vacancy model. The actual measured value was 4.391 gms/cc, which is about 0.9 percent lower than the value calculated for anion vacancies, and 2.0 percent lower than the value calculated for cation interstitials. The value is quite close to the former, but for the above reasons it cannot be stated with absolute certainty which type of defect is present.

TABLE XII

Values of θ_o and θ_1 in °K

	θ_o	θ_1
Kriessman and Harrison	2020	4350
Epstein and Frackiewicz	1920	4200
Current Determination	1850	4510

Anion vacancies are perhaps the easiest type of defect to visualize; ions are simply removed and there are not the geometric restrictions characteristic of the interstitial case. However, the location of interstitial cations on certain vacant lattice sites can be predicted from space limitations. The spinel unit cell which contains eight molecules, has 72 vacant sites that could conceivably contain an interstitial cation. These sites occur at the 8b, 48f, and 16c positions of space group O_h^7. Space considerations would favor the location of the interstitial ions at the 16 c positions. For the case where a = 8. 3848 A, and u = . 381, these sites lie between two cations at 1. 815 A and are surrounded by an irregular octahedron of oxygen ions at 2. 148 A. The tetrahedrally coordinated 8b and 48f sites, on the other hand, have oxygen neighbors at 1. 728 A and 1. 820 A, respectively whereas the sum of the ionic radii, corrected for tetrahedral coordination is 1. 95 A for Mg^{+2} and O^{-2} and about 1. 93 A for Fe^{+3} and O^{-2}.[42, 43] (The occupied 8a sites are compressed, as they are in a number of spinels,[44] and have a separation of 1. 903 A).

The magnetic moments obtained here on non-stoichiometric magnesium ferrite are compared to those obtained on "magnesium ferrite" by Kriessman and Harrison[33] in Fig. 19. Although the temperature dependence of the moments are quite similar, the present results are from 15 to 30 percent higher than those obtained by the latter authors. This is due in part to the difference in composition and the very sensitive dependence of the cation distribution on composition. It demonstrates clearly why the results of various investigators in the past have differed. The phase changes accompanying temperature and atmosphere variations discussed previously[25] make direct comparisons between investigators difficult if not impossible. Most significant is the fact that equimolar mixtures of MgO and Fe_2O_3 do not form $MgFe_2O_4$ at elevated temperatures, but rather an oxygen deficient structure similar in oxygen content to that reported here. At low temperatures, the composition prepared from MgO + Fe_2O_3 will continuously decompose to finally form Fe_2O_3 + $(MgO)_{0.092}MgFe_2O_4$. This system has been perhaps the most complicated of all spinel systems to describe because of the complexity of the phase relations, the temperature and composition dependence of the cation distribution, and finally, the very long times to reach true chemical and ionic equilibrium.

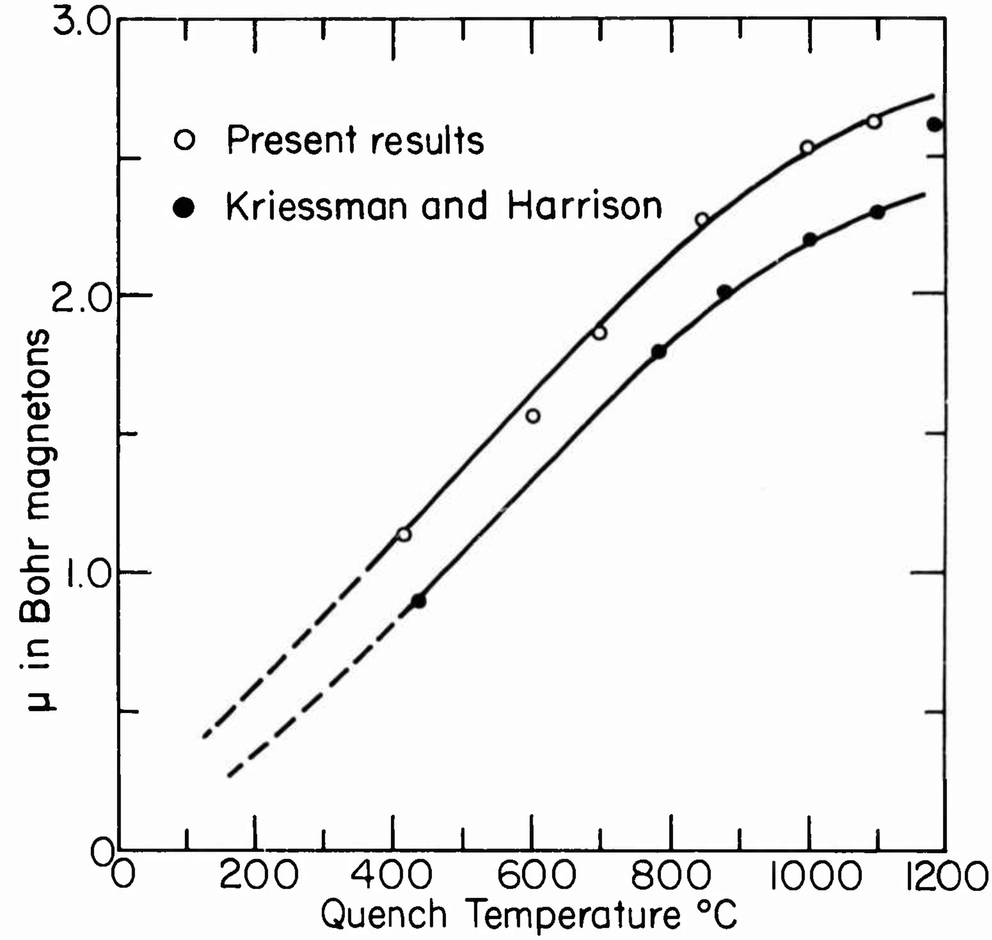

MAGNETIC MOMENT OF MAGNESIUM FERRITE
AS A FUNCTION OF QUENCH TEMPERATURE
FIGURE 19

D. Electrical Conductivity in Nickel Ferrous Ferrites

1. Introduction

In an earlier report,[1] a simple analysis of the conduction process in magnetite derived spinels was developed. For high ferrous ion concentrations in $Ni^{+2}_{1-x}Fe^{+2}_{x}Fe^{+3}O_4$, i.e., $x > 0.2$, the electron hopping from one octhedral site to another could be described in a manner analogous to a diffusion process. By considering the mean time of stay of an electron on an octhedral site, the hopping over the potential barrier separating adjacent ferric ions was described as an activated process characterized by an activation energy, E. By combining the expression for the diffusion coefficient of a hopping electron with the mobility for a charged particle described by the Nernst-Einstein relationship, the temperature dependence of the electrical conductivity for constant charge carriers was formulated. At small values of x and at high temperature, the number of thermally generated intrinsic carriers was considered to become significant compared to the number of temperature independent carriers which is fixed by composition. The statistical problem of distributing electrons between the Ni^{+2} and Fe^{+2} sites was considered, and it was possible to determine the temperature dependence of the number of charge carriers. Combining this result with the previous one describing the temperature dependence of electron hopping, the overall temperature dependence of the electrical conductivity was predicted.

Measurements were made on a series of samples and the results were in good agreement with the predictions of the theory. However, there were several inconsistencies between material prepared at different times, which did not allow for placing complete confidence in the proposed model. The main limitation in preparing dense samples was the necessity of quenching known compositions from elevated temperatures. This undoubtedly introduced cracks, and it could never be certain whether the desired composition was preserved. Very small spheres were prepared in this manner, and could not be checked with lattice parameter measurements (the lattice constant varies linearly between $NiFe_2O_4$ and Fe_3O_4[1]). A large effort was made during the past year to

develop a method of sample preparation that would reduce the amount of phase equilibria information required and at the same time prepare dense, coherent samples of explicitly defined composition.

2. Sample Preparation

The ternary system FeO-NiO-Fe_2O_3 was described in detail in the last final report.[1] It was shown that the CO_2 isobar was located along the Fe_3O_4-$NiFe_2O_4$ join for temperatures above 1300°C. This isobar does not emerge out of the spinel field very far from nickel ferrite, so that it can be used to prepare quenched powders of single phase compositions between Fe_3O_4 and $NiFe_2O_4$. In CO_2, solid solutions from Fe_3O_4 to x equal to 0.10 and 0.15 were prepared at 1300°C and 1500°C, respectively.

Dense samples having the stoichiometric spinel oxygen fraction of 4/7 were prepared using a Maur automatic recording thermobalance with the gas mixing apparatus described earlier. The gas apparatus varied the ambient atmosphere in the furnace from one atmosphere of oxygen to a partial oxygen pressure of 1×10^{-10} atmosphere.

Five-gram samples of the quenched stoichiometric powders were hydrostatically pressed, suspended from one pan of the balance, and lowered into the furnace. The furnace was heated to the sintering temperature (1300°C to 1500°C) and any changes in weight noted on the chart recording caused by oxygen gain or less were compensated for by adjusting the oxygen pressure in the appropriate direction to maintain the initial weight of the sample. At temperature, the correct atmosphere obtained from the phase diagram was passed through the furnace. The samples were sintered for 48 hours, the temperature was lowered, and any changes of weight were again corrected for by changing the ratio of CO_2 to CO.

A section of the top and bottom of the sintered cylinders was removed and lattice parameters determined. The X-ray data showed the samples to be single phase spinels and the lattice parameter values on the top and bottom

of the sintered cylinder were in excellent agreement with the values obtained in the phase equilibria studies.[1] Densities of the sintered cylinders were above 90 percent of theoretical values.

This technique circumvents the need for defining phase relations over very wide limits of temperature, pressure, and composition, and should be applicable to other systems where oxidation states in fixed ratios are required.

3. Results and Discussion

Measurements of electrical conductivity vs temperature were carried out on a set of high density nickel ferrous ferrites between 220° and 475°K. The measurements were made at 10 Gc by the eddy current method.[45, 46] The results are shown in Fig. 20 in which the resistivity divided by the temperature is plotted vs the reciprocal temperature. These results are qualitatively similar to those previously reported[1, 47] on an earlier set of less dense samples, and the same type of analysis has been applied. The analysis is based on the model of thermally activated electron hopping between octhaedral iron sites with a mean time of stay given by $\tau = \tau_o e^{E/kT}$, where E is the activation energy. From diffusion theory one readily predicts a resistivity given by

$$\rho = \text{const} \frac{T}{n} \exp(E/kT) \quad ,$$

where n is the carrier density. If n is constant with temperature, a plot of ρ/T vs $1/T$ as in Fig. 20 should be a straight line whose slope allows computation of the activation energy. The experimental data for x = 0. 4 to x = 0. 9 have been fitted with straight lines in Fig. 20 and the corresponding activation energies are tabulated in Table XIII. However, the assumption of constant n may not be valid for the combination of high temperature and small x value. Under these conditions it is possible that the number of carriers may be significantly altered by the generation of Fe^{+2} - Ni^{+3} pairs. If the Fe^{+2} energy level (the energy of an electron when attached to an Fe^{+2} ion) lies above the Ni^{+2} energy level (the energy of an electron when attached to

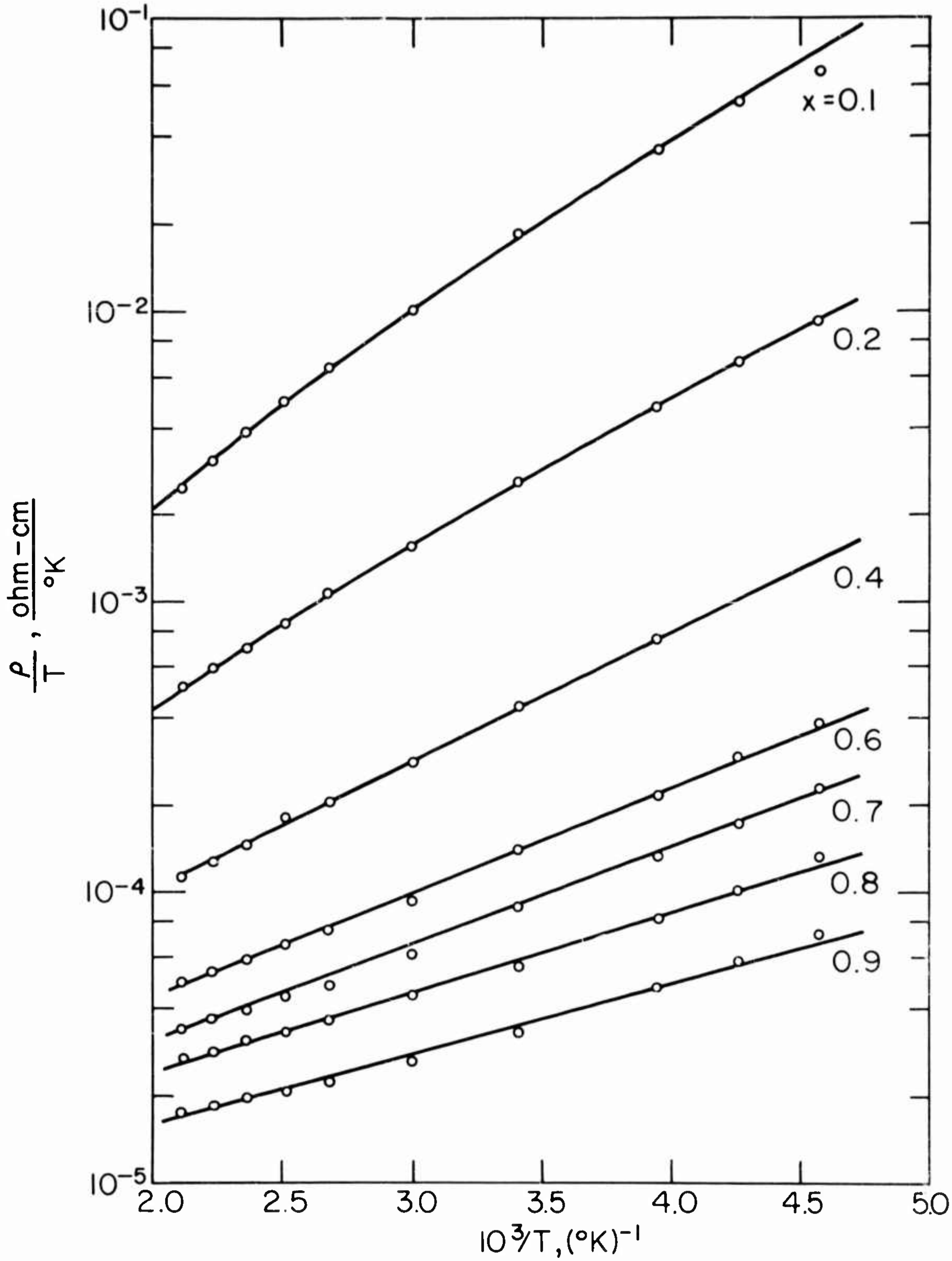

RESISTIVITY AS A FUNCTION OF RECIPROCAL TEMPERATURE FOR VARIOUS X VALUES IN $Ni^{2+}_{1-x}Fe^{2+}_{x}Fe^{3+}_{2}O_4$

FIGURE 20

TABLE XIII

Activation Energies for Electrical Conductivity in

$Ni^{+2}_{1-x}Fe^{+2}_{x}Fe^{+3}O_4$

x	E, ev
0.1	0.10
0.2	0.095
0.4	0.088
0.6	0.071
0.7	0.065
0.8	0.054
0.9	0.048

a Ni^{+2} ion) by an amount 2Δ, the number of Fe^{+2} ions is given by

$$n_{Fe} = \frac{N(1 + x)}{e^{(\Delta - \epsilon)/kT} + 1}$$

where N is the number of moles of $Ni_{1-x}Fe_{2+x}O_4$ and $\Delta - \epsilon$ is the height of the Fe^{+2} level above the Fermi level. If conduction due to holes is neglected, the resistivity becomes

$$\rho = \text{const } T \exp(E/kT) \,[\exp(\Delta - \epsilon)/kT + 1] \quad .$$

The solid curves in Fig. 20 for x = 0.1 and 0.2 were computed using Δ = 0.08 ev and the activation energies listed in Table XIII It may be seen that the theoretical curves agree well with the experimental values. The curve for x = 0.2 has much less curvature than for x = 0.1. For values of x larger than 0.2, the carrier density does not change significantly over the experimental temperature range and the equations become indistinguishable

Thus, the general features of the resistivity data are consistent with the model of thermally activated electron hopping between iron ions, with a separation of the Fe^{+2} and Ni^{+2} energy levels of 0 16 ev

IV. SUMMARY

During the three years of research conducted under the present contract, an effort has been made to describe in detail the chemistry, or phase equilibrium relationships, in magnetic systems of both practical and theoretical interest. The point of view has been first, to understand the chemistry in systems that are considerably more complex than non-condensed systems, and second, to prepare exact compositions of single crystals in garnet systems, and polycrystalline samples in spinel systems. In the garnet systems, the knowledge of the phase relations was a necessary precursor to crystal growth because of the strong dependence of liquidus compositions and crystallization behavior on temperature and oxygen pressure. In spinel systems, phase equilibria relationships had to be determined so that solid solutions of precisely defined ferrous ion concentrations could be prepared. Perhaps no single property of transition element oxides depends more strongly on composition than the electrical conductivity. By very careful preparation of samples in one system, meaningful results have been obtained and a possible explanation made regarding the somewhat unexpected temperature dependence of the conductivity for certain compositions. The long held view that the conductivity losses in ferrites is caused by the ferrous ion concentration fixed by composition may be overly restrictive.

In final summary, the papers being prepared and already published based on work performed under this contract are listed below.

PUBLICATIONS

1. H. J. Van Hook, "Phase Relations in the System Fe_2O_3-Fe_3O_4-$YFeO_3$ in Air," J. Am. Ceram. Soc. 44, [5] 208-214 (1961).

2. H. J. Van Hook, "Phase Relations in the Ternary System Fe_2O_3-FeO-$YFeO_3$," J. Am. Ceram. Soc. 45, [4] 162-165 (1962).

3. H. J. Van Hook, "Phase Equilibrium Studies in the System Iron Oxide-Y_2O_3-Gd_2O_3," J. Am. Ceram. Soc. 45 (August 1962).

4. B. D. Roiter and A. E. Paladino, "Phase Equilibria in the Ferrite Region of the System Fe-Co-O," J. Am. Ceram. Soc. 45, [3] 128-133 (1962).

5. T. Kohane and B. D. Silverman, "Electrical Conduction in Nickel Ferrous Ferrites," J. Phys. Soc. (Japan Notes) 17, 249 (1962).

PAPERS BEING PREPARED FOR PUBLICATION

1. "Phase Relations in the Garnet Region of the System Fe_2O_3-FeO-Al_2O_3-Y_2O_3."

2. "Crystal Growth of the Magnetic Garnets by the Czochralski Technique."

3. "The System $NiFe_2O_4$-Fe_3O_4."

4. "Phase Equilibria in the System FeO-Fe_2O_3-Al_2O_3."

5. "Cation Distribution in Non-Stoichiometric Magnesium Ferrite."

ACKNOWLEDGMENT

The authors would like to acknowledge the assistances of Messrs. C. R. Snider, R. B. Hawkes, M. E. Nichols and F. M. Golden, and Miss S. Georgian in the experimental work and Dr. B. D. Silverman for discussions on conductivity mechanisms. Miss C. A. Lyons is particularly acknowledged for her patience in typing this report from the illegible writings of the authors.

REFERENCES

1. Raytheon Company, "Research on the Chemistry and Single Crystal Growth of Magnetic Oxides," Final Report, AF 19 (604)-5511 (June 5, 1961).

2. J. W. Nielsen and E. F. Dearborn, "The Growth of Single Crystals of Magnetic Garnets," J. Phys. Chem. Solids 5, 202-207 (1958).

3. R. G. Rudness and R. W. Kebler, "Growth of Single Crystals of Incongruently Melting Yttrium Iron Garnet by the Flame Fusion Process," J. Am. Ceram. Soc. 43, [1] 17-22 (1960).

4. International Telephone and Telegraph Laboratories, "Research on Growing Crystals of Ferrimagnetic Oxides," Scientific Report No. 7, AF 19 (604)-2261 (June 1, 1959).

5. L. L. Abernethy, J. H. Ramsey, and J. W. Ross, "Growth of Yttrium Iron Garnet Single Crystals by the Floating Zone Technique," J. Appl. Phys. 32, 376S-377S (1961).

6. S. Geller, "Magnetic Interactions and Distributions in the Garnets," J. Appl. Phys. 31, 30S-37S (1960).

7. I. Warshaw and R. Roy, "Stable and Metastable Equilibria in the System Y_2O_3-Al_2O_3 and Gd_2O_3-Fe_2O_3," J. Am. Ceram. Soc. 42, [9] 434-438 (1959).

8. F. Bertaut and F. Forrat, "Structure des Ferrites Ferrimagnetiques des Terres Rares," Compt. rendus. 242, 382-384 (1956).

9. H. J. Van Hook, "Phase Equilibrium Studies in the System Iron Oxide-Y_2O_3-Gd_2O_3," J. Am. Ceram. Soc. 45 (August 1962).

10. S. Geschwind, "Paramagnetic Resonance of Fe^{+3} in Octahedral and Tetrahedral Sites in Yttrium Gallium Garnet (YGaG) and Anisotropy of Yttrium Iron Garnet (YIG)," Phys. Rev. 121, [2] 363-374 (1961).

11. E. A. Maguire, "Ceramic and Magnetic Properties of Substituted Yttrium Iron Garnet of the Type $Y_3Fe_{5-x}M_xO_{12}$," Raytheon Memo T-227 (June 14, 1960).

12. H. J. Van Hook, "Phase Relations in the Ternary System Fe_2O_3-FeO-$YFeO_3$," J. Am. Ceram. Soc. 45, [4] 162-165 (1962).

13. A. Muan and C. L. Gee, "Phase Equilibrium Studies in the System Iron Oxide-Al_2O_3 in Air and at 1 Atmosphere O_2 Pressure," J. Am. Ceram. Soc. 39, [6] 207-214 (1956).

14. R. G. Richards and J. White, "Phase Relationships of Iron Oxide Containing Spinels," Part I. Trans. Brit. Ceram. Soc. 53, [4] 233-270 (1954).

15. L. M. Atlas and W. K. Sumida, "Solidus, Subsolidus, and Sub-dissociation Phase Equilibria in the System Fe-Al-O," J. Am. Ceram. Soc. 41, [5] 150-160 (1958).

16a. A. Muan, "Phase Equilibria at High Temperatures in Oxide Systems Involving Changes in Oxidation States," Am. J. Sci. 256, 171-207 (March 1958);

b. A. Muan, "Phase Equilibria in the System FeO-Fe_2O_3-SiO_3," J. of Metals, 1-12 (September 1955).

17. W. H. Bauer and I. Gordon, "Flame-Fusion Synthesis of Several Types of Silicate Structures," J. Am. Ceram. Soc. 34, [8] 250-254 (1951).

REFERENCES (Continued)

18. B. Chalmers, "Melting and Freezing," Trans. AIME 200, 519-532 (1954).

19. T. B. Reed, "Plasma Torches," Science and Technology 1, [6] 42-48 (1962).

20. H. E. Buckley, CRYSTAL GROWTH, John Wiley and Sons, Inc., New York (1951).

21. Airtron, Inc., "The Preparation of Single Crystal Ferrite Materials by the Floating Zone Technique," Twelfth Quarterly Report NORD 18020 (February 10, 1961).

22. F. R. Monforte, F. W. Swanekamp, and L. G. Van Uitert, "Radio Frequency Technique for Pulling Oxide Crystals Without Employing a Crucible Susceptor," J. Appl. Phys. Letters 32, [5] 959 (1961).

23. A. E. Paladino, "Phase Equilibria in the Ferrite Region of the System Fe-Ni-O," J. Am. Ceram. Soc. 42, [4] 168-175 (1959).

24. B. D. Roiter and A. E. Paladino, "Phase Equilibria in the Ferrite Region of the System Fe-Co-O," J. Am. Ceram. Soc. 45, [3] 128-133 (1962).

25. A. E. Paladino, "Phase Equilibria in the Ferrite Region of the System FeO-MgO-Fe_2O_3," J. Am. Ceram. Soc. 43, [4] 183-191 (1960).

26. W. D. Kingery, J. Pappis, M. E. Doty, and D. C. Hill, "Oxygen Ion Mobility in Cubic $Zr_{0.85}Ca_{0.15}O_{1.85}$," J. Am. Ceram. Soc. 42, [8] 393-398 (1959).

REFERENCES (Continued)

27. A. Hoffman and W. A. Fischer, "Bilding des Spinels FeO · Al_2O_3 and Seiner Mischkristalle mit Fe_3O_4 and Al_2O_3," Zeitchr. Phys. Chem. Neue Folge 1, 80-90 (1956).

28. T. F. W. Barth and E. Posnjak, "Spinel Structure With and Without Variate Atom Equipoints," Zeits. f. Krist 82, 325 (1932).

29. E. F. Bertaut, "Some Recent Progress in Crystallography of Spinels, in Particular of the Ferrites," J. Phys. Radium 12, 252-255 (1951).

30. G. E. Bacon and F. F. Roberts, "Neutron Diffraction Studies of Magnesium Ferrite Aluminate Powders," Acta Cryst. 6, [1] 57-62 (1953).

31. L. M. Corliss, J. M. Hastings, and F. G. Brockman, "Neutron-Diffraction Study of Magnesium Ferrite," Phys. Rev. 90, [6] 1013-1018 (1953).

32. Réne Pauthenet and L. Bochirol, "Spontaneous Magnetizations of Some Ferrites," J. Phys. Radium, 12, [3] 249-251 (1951).

33. C. J. Kriessman and S. E. Harrison, "Cation Distributions in Ferrospinels: Magnesium-Managanese Ferrites," Phys. Rev. 103, [4] 857-860 (1956).

34. D. J. Epstein and B. Frackiewicz, "Some Properties of Quenched Magnesium Ferrites," J. Appl. Phys. 29, [3] 376-377 (1958).

35. S. Foner, "Versatile and Sensitive Vibrating-Sample Magnetometer," Rev. Sci. Instr. 30, [7] 548-557 (1959).

REFERENCES (Continued)

36. H. P. Klug and L. E. Alexander, X-RAY DIFFRACTION PROCEDURES, Chapter 5, John Wiley and Sons, Inc., New York (1954).

37. J. Berghius et al., "New Calculations of Atomic Scattering Factors," Acta Cryst. 8, 478 (1955).

38. R. E. Watson and A. J. Freeman, "Hartree-Fock Atomic Scattering for the Iron Transition Series," Acta Cryst. 14, 27 (1961).

39. Private communication from A. J. Freeman to O. J. Guentert.

40. L. G. Parratt and C. F. Hempstead, "Anomalous Dispersion and Scattering of X-Rays," Phys. Rev. 94, 1593 (1954).

41. H. B. Callen, S. E. Harrison, and C. J. Kriessman, "Cation Distributions in Ferrospinels. Theoretical," Phys. Rev. 103, 851 (1956).

42. L. Pauling, THE NATURE OF THE CHEMICAL BOND, 2nd edition, Cornell University Press, Ithaca, New York (1948).

43. L. H. Ahrens, "Use of Ionization Potentials. I. Ionic Radii of the Elements," Geochim et Cosmochim. Acta 2, 155-169 (1952).

44. E. W. Gorter, "Ionic Distribution Deduced from the g-factor of a Ferrimagnetic Spinel: Ti^{4+} in Four-Fold Coordination," Nature 174, 123 (1954).

45. T. Kohane and M. H. Sirvetz, "Measurement of Microwave Resistivity by Eddy Current Loss in Spheres," Rev. Sci. Instr. 30, 1059 (1959).

REFERENCES (Continued)

46. T. Kohane, "The Measurement of Microwave Resistivity by Eddy Current Loss in Small Spheres," IRE Trans. on Instr. I-9, 184 (1960).

47. T. Kohane and B. D. Silverman, "Electrical Conduction in Nickel Ferrous Ferrites," J. Phys. Soc. Japan 17, 249 (1962).